

# Critical Tests Of The Leading Gamma Ray Burst Theories

Shlomo Dado and Arnon Dar

*Physics Department, Technion, Haifa 32000, Israel*

## Abstract

Although it has been established observationally beyond doubt that broadline stripped envelope supernovae (SNe) of type Ic produce long duration gamma ray bursts (GRBs), that neutron star mergers produce short hard GRBs (SHBs), and that phase transition of neutron stars in high mass X-ray binaries (HMXBs) may produce SN-Less GRBs, their production mechanism is still debated. The two leading theoretical models of GRBs and their afterglows, the fireball model and the cannonball model, have been widely confronted with the mounting observational data on GRBs and SHBs during the last two decades. Both have claimed success in reproducing the observational data, despite their complexity and diversity. This claimed success, however, may reflect multiple choices and the use of many free adjustable parameters, rather than the true validity of the models. Only confrontation of the key falsifiable predictions of the models with solid observational data can test their validity. Such critical tests are reviewed in this report.

PACS numbers: 98.70.Rz, 98.38.Fs

## I. INTRODUCTION

Gamma-ray bursts (GRBs) are brief flashes of gamma rays lasting between few milliseconds and several hours from extremely energetic cosmic explosions [1]. They were first detected on July 2, 1967 by the USA Vela spy satellites, which were launched to detect USSR tests of nuclear weapons above the atmosphere, in violation of the USA-USSR Nuclear Test Ban Treaty signed in 1963. Their discovery was first published in 1973 after 15 such events were detected [2], which have ruled out man-made origin and indicated that they were outside the solar system.

During the first 20 years after their discovery, hundreds of models of GRBs were published (see, e.g., [3]), where it was assumed that GRBs are Galactic in origin. An extragalactic origin implied implausible energy release in gamma rays from a very small volume in a very short time, if they were isotropic, as was generally assumed. During that period it was also found that GRBs fall roughly into two classes, long duration ones (LGRBs) that last more than  $\sim 2$  seconds, and short bursts (SGRBs) that typically last less than  $\sim 2$  seconds [4] most of which are short hard bursts (SHBs) with a spectrum much harder than LGRBs. The origin and production mechanism of both types of GRBs have been major astrophysical puzzles until recently.

In 1984, Blinnikov et al. [5] suggested that exploding neutron stars in close binaries may produce GRBs with isotropic gamma ray energy that could reach  $\sim 10^{46}$  erg. Such GRBs could be seen only from relatively nearby galaxies. Paczynsky, however, maintained [6] that the sky distribution of GRBs is more consistent with large cosmological distances, like those of quasars, with a redshift of about 1 or 2, which implies a release of supernova-like energy,  $\sim 10^{51}$  erg, within less than 1 s, making gamma-ray bursters the brightest objects known in the universe, many orders of magnitude brighter than any quasar [6].

The first plausible physical model of extragalactic gamma-ray bursts at large cosmological distances, was proposed by Goodman, Dar and Nussinov in 1987 [7]. They suggested that extragalactic GRBs may be produced in stripped envelope supernova explosions (SNe) and in neutron stars mergers by an  $e^+e^-\gamma$  fireball [8] formed by neutrino-antineutrino annihilation around the newly born compact object – a massive neutron star ( $n^*$ ) or a black hole (bh). But shortly after the launch of the Compton Gamma-Ray Burst Observatory (CGRO) in 1991, it became clear that such neutrino-annihilation fireballs are not powerful enough to

produce observable GRBs at the very large cosmological distances, which were indicated by the CGRO observations [9], unless the produced  $e^+e^-\gamma$  fireballs are collimated by funneling through surrounding matter into a conical fireball [10]. Shaviv and Dar, however, suggested instead [11] that narrowly beamed GRBs can be produced by jets of highly relativistic plasmoids (cannonballs) of ordinary matter through inverse Compton scattering (ICS) of light surrounding their launch sites. They proposed that such jets may be launched in stripped-envelope core-collapse supernova explosions, in merger of compact stars due to the emission of gravitational waves, and in phase transition of neutron stars to a more compact object, i.e., a quark star ( $q^*$ ) or a black hole (bh), following mass accretion in compact binaries.

An important prediction of the fireball model was a transition of the initial short  $\gamma$ -ray emission to emission of a longer-lived "afterglow" [12] at longer wavelengths due to the slow down of the expansion of the  $e^+e^-\gamma$  fireball by the swept in surrounding medium. In 1997, measurements with the Italian-Dutch satellite BeppoSAX discovered that GRBs are indeed followed by a longer-lived X-ray "afterglow" [13]. It provided accurate enough sky localization of GRBs, which led to the discovery of their afterglow at longer wavelengths [14], the discovery of their host galaxies [15] and their redshifts [16] shortly after, and the association of long GRBs with supernova (SN) explosions of type Ic [17]. Following measurements during the past 20 years, mainly with the X-ray satellites HETE, Swift, Konus-Wind, Chandra, Integral, XMM-Newton, and Fermi, the Hubble space telescope, and ground based telescopes, provided the detailed properties of the prompt and afterglow emissions of GRBs over the entire electromagnetic spectrum, the association of LGRBs with SNeIc and the properties of their host galaxies and near environments [18]. In particular, they provided clear evidence that LGRBs are taking place mainly in star formation regions within the disk of spiral galaxies, where most SNeIc take place, while SGRBs are taking place in and outside of both spiral and elliptical galaxies. This suggested a different origin of LGRBs and SGRBs. While LGRBs were observed to be associated with SNeIc, SHBs were not. That, and the location of SHBs led to the wide spread belief that SHBs are produced in merger of neutron stars, and/or a neutron star and a black hole [7,10] in close binaries.

This belief was based on indirect evidence [19]. Recently, however, SHB170817A [20] that followed  $1.74 \pm 0.05$  s after the gravitation wave (GW) chirp from a relatively nearby

neutron stars merger (NSM) event, GW170817, which was detected with the Ligo-Virgo GW detectors [21], has shown beyond doubt that neutron star mergers produce SHBs. Moreover, the universal shape of all the well sampled early time afterglow of ordinary SHBs and of SHB170817A [22], which is expected from a pulsar wind nebula (PWN) emission powered by the spin down of a newly born milli second pulsar (MSP), suggest that most SHBs, are produced by NSMs yielding a neutron star remnant rather than a stellar mass black hole [22].

Although long duration nearby GRBs have been seen in association with very bright broad-line supernova explosions of type Ic [17,23], no associated SN has been detected in several nearby long duration GRBs despite very deep searches [24]. The universal behavior of the afterglow of such long duration SN-Less GRBs and SHBs [22, 25], however, suggest that they are also powered by a newly born millisecond pulsars, perhaps in phase transition of neutron stars to quark stars [11,26] following mass accretion onto neutron stars in high mass X-ray binaries (HMXBs).

Since 1997 only two theoretical models of GRBs and their afterglows, the standard fireball (FB) model [27] and the cannonball (CB) model [28], have been used extensively to interpret the mounting observational data on GRBs and their afterglows. Both models have claimed to reproduce well the observational data. But, despite their similar names, the two models were originally and still are very different in their basic assumptions and predictions. This is despite the replacement of key assumptions underlying the standard FB models with assumptions underlying the CB model (see below). The claimed success, however, of both models in reproducing the mounting observational data on GRBs and their afterglows, despite the complexity and diversity of these data, may reflect the fact that the predictions of both models depend on free parameters and choices, which, for each GRB, were adjusted to fit the observational data. As a result, when successful fits to observational data were obtained, it was not clear whether they were due to the validity of the theory or due to multiple choices and the use of many adjustable parameters to describe individual GRBs and their afterglows.

Scientific theories, however, must be falsifiable [29]. Hence, only confrontations between key predictions of the GRB models, which do not depend on free adjustable parameters, with solid observational data can serve as critical tests of the validity of such models, rather than biases, prejudices, consensus or beliefs. Such critical tests of the cannonball model

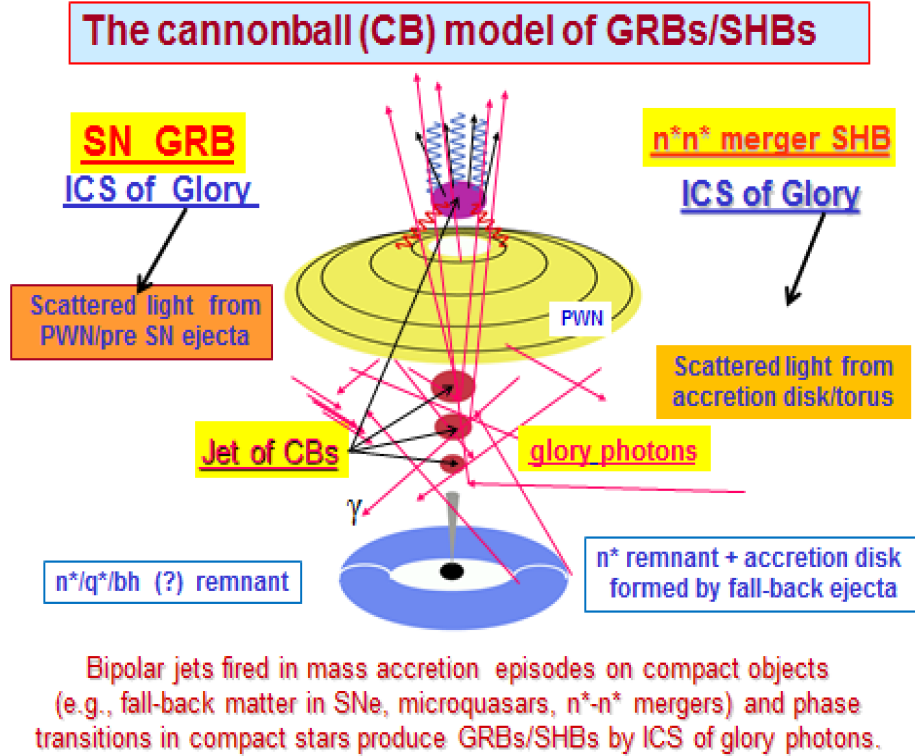


FIG. 1: Schematic description of the CB model of GRBs

and the standard fireball model of long GRBs and SHBs are reviewed in this report. The obvious conclusion is left to be drawn by the unbiased reader.

## II. THE GRB MODELS

GRBs and SHBs seem to consist of a few short  $\gamma$ -ray pulses with roughly a fast rise and an exponential decay (FRED) pulse-shape [1]. The number of such individual pulses, their time sequence, relative intensities, and durations, that vary drastically from burst to burst and within bursts, are not predicted by the GRB models. The main properties of resolved pulses, however, such as pulse-shape, polarization and correlations between their main properties, as well as global properties of the entire bursts, and their afterglows are predicted by the models and can be used for critical tests of the modes. Since LGRBs and SGRBs have different progenitors we shall discuss the critical tests of their CB and FB models separately. **The CB model** [28,30,26,25], is illustrated in Figure 1. In the CB model, bipolar jets of highly relativistic plasmoids (cannonballs) are assumed to be launched by fall back material onto the newly born compact stellar object [11], a neutron star, a quark

star or a black hole in stripped envelope supernovae explosions of type Ic (SN-GRBs), in NSM in close binaries (SHBs), and in phase transition of neutron stars to  $q^*$  due to mass accretion (SN-less GRBs) in HMXBs. The prompt emission  $\gamma$ -ray pulses are produced by ICS of the radiation (glory) surrounding the launch site, by the electrons enclosed in the CBs of the jet. In SN-GRBs, this glory can be the light halo formed around the progenitor star by scattered light from pre-supernova ejections. In SN-less GRBs it can be light from the massive star companion, or the radiation emitted from the accretion disk formed around the neutron star. In SHBs it can be the X-ray radiation from an accretion disk formed around the  $n^*$ 's remnant by fall back of tidally disrupted material or debris from the final explosion of the lighter  $n^*$  [5] after losing most of its mass.

When the CBs enter the interstellar medium, they decelerate by sweeping in the ionized medium in front of them. The swept in electrons and nuclei are Fermi accelerated there to very high energies by the turbulent magnetic fields present/generated in the CBs. The accelerated electrons cool mainly by emitting synchrotron radiation, which dominates the afterglow of SN-GRBs that usually take place in dense stellar regions - molecular clouds where most SNe take place.

The afterglows of SN-less GRBs and SHBs, which are usually produced in much lower density environments than those of SN-GRBs, appear to be dominated by the radiation from a pulsar wind nebula, which is powered by the spin down of the newly born millisecond pulsar [25,26].

**The FB models of GRBs** evolved a long way from the original spherical  $e^+e^-\gamma$  fireballs [8] formed around stripped envelope supernova explosions [7],  $n^*n^*$  mergers [7] and  $n^*bh$  mergers [10] to the current collimated fireball models [27]. The most popular version is illustrated in Figure 2 adapted from [31]. It assumes that long GRBs are produced by highly relativistic conical jets of ordinary matter launched by collapsars - the collapse of a massive star to a black hole, either directly without a supernova ("failed supernova") [32, 33], or indirectly in a hypernova (the delayed collapse of the newly born compact object to a black hole by mass accretion of fall back material in core collapse supernova explosion[34]). SHBs are assumed to be produced by highly relativistic jets launched in  $n^*n^*$  and  $n^*bh$  mergers.

In the FB models, the prompt emission pulses are assumed to be produced by synchrotron

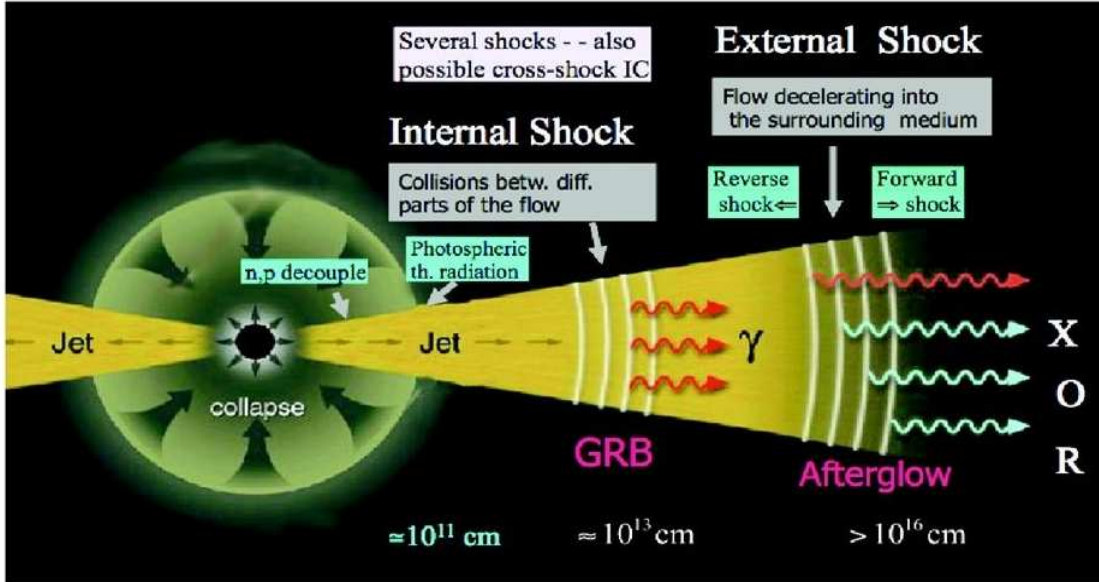


FIG. 2: Schematic description of the fireball model of GRBs adapted from a recent review of GRBs by Meszaros and Rees [31].

radiation emitted by highly relativistic electrons shock accelerated in the collisions between overtaking conical shells. The continuous collision of the merged shells with the circumburst medium is assumed to drive a forward shock into the interstellar medium or pre-ejected stellar wind, and a reverse shock into the merged shells. The shock accelerated electrons produce synchrotron radiation (SR) afterglow [27] on top of a hypernova [34] light in LGRBs, or a macronova light in SHBs [35]. The reverse shock produces the optical photons while inverse Compton scattering of the SR in the forward blast wave produce GeV-TeV photons.

### III. PROMPT EMISSION TESTS

#### Test 1: Polarization.

**In the CB model**, ordinary GRBs are produced by narrowly collimated jets of CBs with a bulk motion Lorentz factor  $\gamma_0 = \gamma(t=0) \gg 1$  through inverse Compton scattering of light. They are narrowly beamed and are viewed from small angles  $\theta \approx 1/\gamma_0 \ll 1$  relative to the jet direction of motion, i.e., with Doppler factors  $\delta_0 = \delta(t=0) = 1/\gamma_0(1 - \beta \cos\theta) \approx 2\gamma_0/(1 + \gamma_0^2\theta^2)$  to a good approximation for  $\gamma_0^2 \gg 1$ , and  $\theta^2 \ll 1$ . For the most probable viewing angles

$\theta \approx 1/\gamma_0$  of such GRBs, their expected linear polarization is [36]:

$$\Pi = 2\gamma_0^2 \theta^2 / (1 + \gamma_0^4 \theta^4) \approx 100\%. \quad (1)$$

High luminosity (HL) GRBs, or low luminosity (LL) GRBs, that in the CB model are mainly GRBs viewed from very near axis ( $\gamma_0^2 \theta^2 \ll 1$ ), or very far off-axis ( $\gamma_0^2 \theta^2 \gg 1$ ), respectively, are expected to display a small linear polarization. For instance,  $\Pi < 0.22$  is predicted for HL GRBs with  $\gamma_0 \theta < 1/3$ , and for LL GRBs with  $\gamma_0 \theta > 3$ . However, HL or LL GRBs that are very bright or very dim, respectively, because of having an unusual very large or very small  $\gamma_0$ , respectively, and are viewed from  $\theta \approx 1/\gamma_0$ , are expected to display a rather large polarization.

**In the standard FB models**, GRB pulses are produced by synchrotron radiation emitted by high energy electrons, which are Fermi/shock accelerated in collisions between conical shells or by shocks within conical flows (jets). Such Fermi/shock acceleration, however, requires highly turbulent magnetic fields in the acceleration region, which produce a very small net polarization. Indeed, the afterglow of GRBs, that in both the CB model and the FB models is produced by synchrotron emission from shock accelerated electrons, is observed to have a very small polarization [37]. This is in contrast to the linear polarization of the prompt emission, which has been found to be very large in all GRBs where it was measured [38], as summarized in Table I. Soon after the first report of a measurement of a large polarization of the prompt emission in a GRB021206, observers questioned the measurement while promoters of firecone/fireshell models proposed posteriori explanations. For instance, it was suggested that a constant magnetic field exists in the small domains of an angular size  $\sim 1/\gamma_0$  of the firecone/fireshell from where the photons arrive simultaneously in the observer frame. However, the observed photons at any given time are a collection of photons, which have the same arrival time, but not the same emission time, i.e., the magnetic field in these different emission domains must align in nearly in the same direction. Such a situation must be present in most GRBs in order to explain the large observed polarization in all cases where it was measured [38]. However, a highly turbulent magnetic field rather than an ordered field is needed in order to Fermi/shock accelerate the electrons to high energy whose emitted synchrotron radiation is assumed to be the GRB prompt emission. Moreover, the above explanations of the observed large polarization [38] are in tension with the curvature effect [39] which was claimed to explain the observed temporal and spectral



TABLE I: GRBs with measured polarization of prompt  $\gamma$ -rays

GRB	Polarization(%)	CL	Reference [38]	Polarimetry
021206	80 +/- 20	???	Coburn & Boggs 2003	RHESSI
930131	> 35,	90%	Willis et al. 2005	BATSE (Albedo)
960924	> 50	90%	Willis et al. 2005	BATSE (ALbedo)
041219A	98 +/- 33	68%	Kalemci et al. 2007	INTEGRAL-SPI
100826A	27 +/- 11	99%	Yonetoku et al. 2011	IKARUS-GAP
110301A	70 +/- 22	68%	Yonetoku et al. 2012	IKARUS-GAP
110721	84 +16/-28	68%	Yonetoku et al. 2012	IKARUS-GAP
061122	> 60	68%	Gotz et al. 2013	INTEGRAL-IBIS
140206A	> 48	68%	Gotz et al. 2014	INTEGRAL-IBIS

behaviors of the prompt emission pulses, and with the relatively small polarization of the afterglow observed right after the prompt emission [37] - an hypothesized constant magnetic field within domains of a size  $\approx 1/\gamma$  would produce also a large polarization during the afterglow phase in contradiction to the small observed polarization.

**Test 2: Correlations.**

**The CB model** entails very simple correlations between the main observables of GRBs [40]. For instance, ICS of glory photons of energy  $\epsilon$  by CBs boosts their energy to  $E_\gamma = \gamma_0 \delta_0 \epsilon / (1 + z)$  in the observer frame. Consequently, the peak energy  $E_p$  of their time-integrated energy distribution satisfies,

$$(1 + z) E_p \propto \gamma_0 \delta_0 \epsilon_p, \tag{2}$$

where  $\epsilon_p$  is the peak energy of the glory. In the Thomson regime, the nearly isotropic distribution of the ICS photons in the CB rest frame (primed) is beamed into a distribution  $dn_\gamma/d\omega = (dn'_\gamma/d\omega) \delta^2 \approx (n_\gamma/4\pi) \delta^2$  in the observer frame. Consequently, the isotropic-equivalent total energy of such scattered photons satisfies

$$E_{iso} \propto \gamma_0 \delta_0^3 \epsilon_p. \tag{3}$$

Hence, both ordinary LGRBs and SGRBs, which in the CB model are GRBs viewed mostly from an angle  $\theta \approx 1/\gamma$ , where  $\delta_0 \approx \gamma_0$ , satisfy similar correlations

$$(1 + z) E_p \propto [E_{iso}]^{1/2}, \tag{4}$$

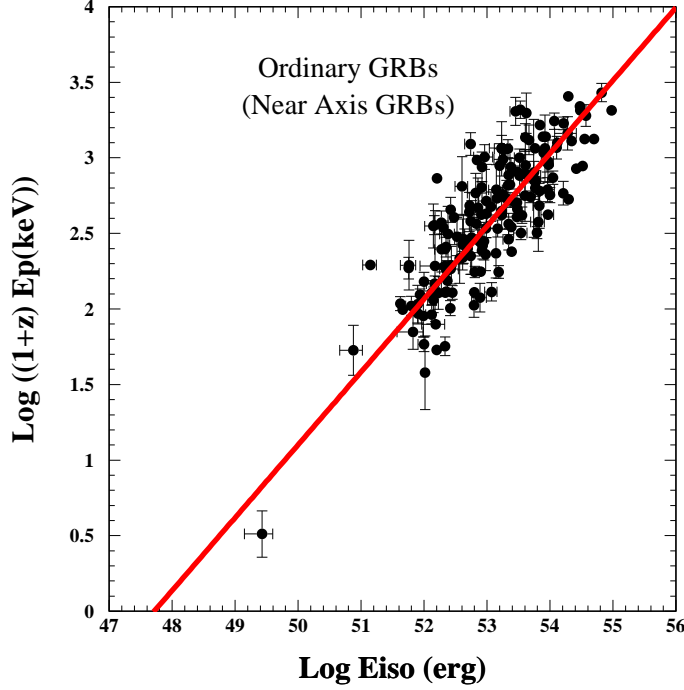


FIG. 3: The  $[E_p, E_{iso}]$  correlation in ordinary LGRBs viewed near axis. The line is the the best fit correlation which is very consistent with the CB model predicted correlation given by Eq.(4).

while far off-axis ones ( $\theta^2 \gg 1/\gamma^2$  and consequently  $\delta_0 \ll \gamma_0$ ) have a much lower  $E_{iso}$ , and satisfy

$$(1+z) E_p \propto [E_{iso}]^{1/3}. \quad (5)$$

These  $[E_p, E_{iso}]$  correlations that were predicted by the CB model [40] and later discovered empirically [41] for ordinary LGRBs are compared in Figures 3,4 to the observational data on GRBs with known redshift. As demonstrated in these figures, the CB model correlations predicted for LGRBs, are well satisfied by both ordinary LGRBs (Eq.(4)) and low luminosity (LL) LGRBs (Eq.(5)). The  $[E_p, E_{iso}]$  correlation predicted by the CB model for LL SGRBs, is also presented in Figure 5. As shown in Figure 5, Eqs.(4) (5) seem to be satisfied by the observational data on SHBs as well.

**The FB models**, have not provided, so far, a plausible derivation of the above well established correlations.

### Test 3: Pulse Shape

GRBs seem to consist of individual short pulses with roughly a fast rise and an exponential

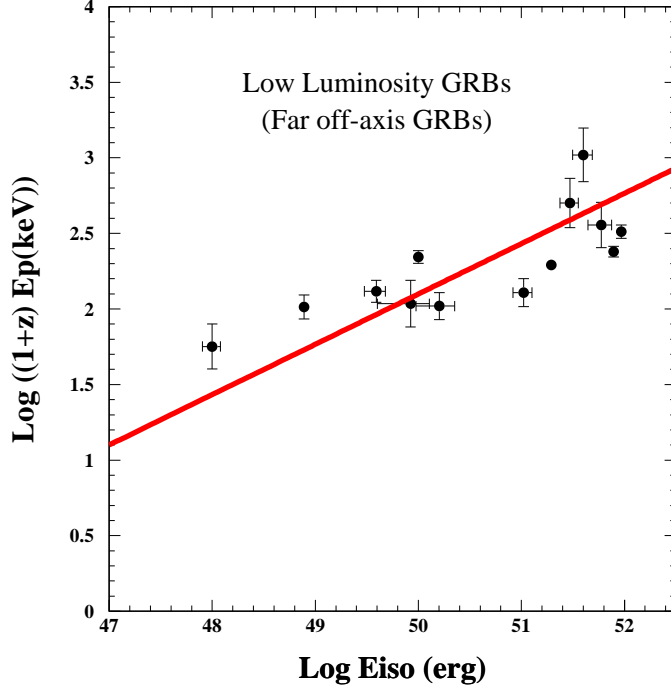


FIG. 4: The  $[E_p, E_{iso}]$  correlation in low luminosity (far off-axis) LGRBs. The line is the CB model predicted correlation as given by Eq.(5).

decay (FRED) pulse shape [1]. Although the number of such pulses, their time sequence, relative intensities and durations that vary drastically between bursts, cannot be predicted by the current GRB models, the typical FRED shape of individual pulses can be predicted. **In the CB model**, the pulse-shape produced by ICS of glory photons with an exponentially cut off power law (CPL) spectrum,  $dn_g/d\epsilon \propto \epsilon^{-\alpha} \exp(-\epsilon/\epsilon_p)$  at redshift  $z$ , by a CB is given approximately [42] by

$$E \frac{d^2 N_\gamma}{dE dt} \propto \frac{t^2}{(t^2 + \Delta^2)^2} E^{1-\alpha} \exp(-E/E_p(t)) \quad (6)$$

where  $\Delta$  is approximately the peak time of the pulse in the observer frame, which occurs when the CB becomes transparent to its internal radiation, and  $E_p \approx E_p(t = \Delta)$ . In eq.(6), the early temporal rise like  $t^2$  is produced by the increasing cross section,  $\pi R_{CB}^2 \propto t^2$ , of the fast expanding CB when it is still opaque to radiation. When the CB becomes transparent to radiation due to its fast expansion, its effective cross section for ICS becomes a constant equal to Thomson cross times the number of electrons in the CB. That, and the density  $n_g$  of the ambient photons, which for a distance  $r = \gamma \delta c t / (1+z) > R_g$  (the radius of the glory)

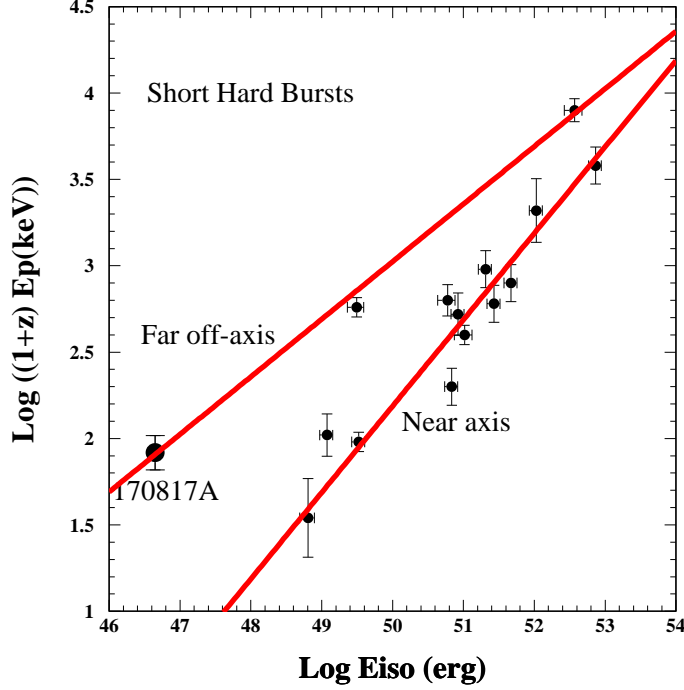


FIG. 5: The  $[E_p, E_{iso}]$  correlations in SHBs. The lines are the CB model predicted correlations as given by Eqs (4) and (5).

decreases like  $n_g(r) \approx n_g(0) (R_g/r)^2 \propto t^{-2}$ , produce the temporal decline like  $t^{-2}$ . If CBs are launched along the axis of a glory of a torus-like pulsar wind nebula, or of an accretion disk with a radius  $R_g$ , then glory photons at a distance  $r$  from the center intercept the CB at a lab angle  $\theta_{int}$ , which satisfies  $\cos \theta_{int} = -r/\sqrt{r^2 + R_g^2}$ . It yields a  $t$ -dependent peak energy,  $E_p(t) = E_p(0)(1 - t/\sqrt{t^2 + \tau^2})$  with  $\tau = R(1+z)/\gamma \delta c$ , and  $E_p \approx E_p(t \approx \Delta)$ , where  $\Delta$  is approximately the peak time of the pulse.

For LGRBs with  $\tau \gg \Delta$ , Eq.(6) yields half maximum values at  $t \approx 0.41 \Delta$  and  $t = 2.41 \Delta$ , which yield a full width at half maximum  $FWHM = 2 \Delta$ , a rise time from half maximum to peak value  $RT = 0.59 \Delta$  and a decay time from peak count to half peak,  $DT = 1.41 \Delta$ . Consequently  $RT/DT \approx 0.42$  and  $RT \approx 0.30 FWHM$ .

The predicted pulse shape as given by Eq.(6) is demonstrated in Figure 6 for the single-pulse of GRB930612, which was measured with BATSE aboard CGRO. In most LGRBs  $\tau \gg \Delta$ . Consequently, the CB model yields for LGRBs a pulse asymmetry ratio  $RT/DT \approx 0.42$ , and  $RT/FWHM \approx 0.29$ . Moreover, these two ratios change very little as long as  $\tau \gg \Delta$ .

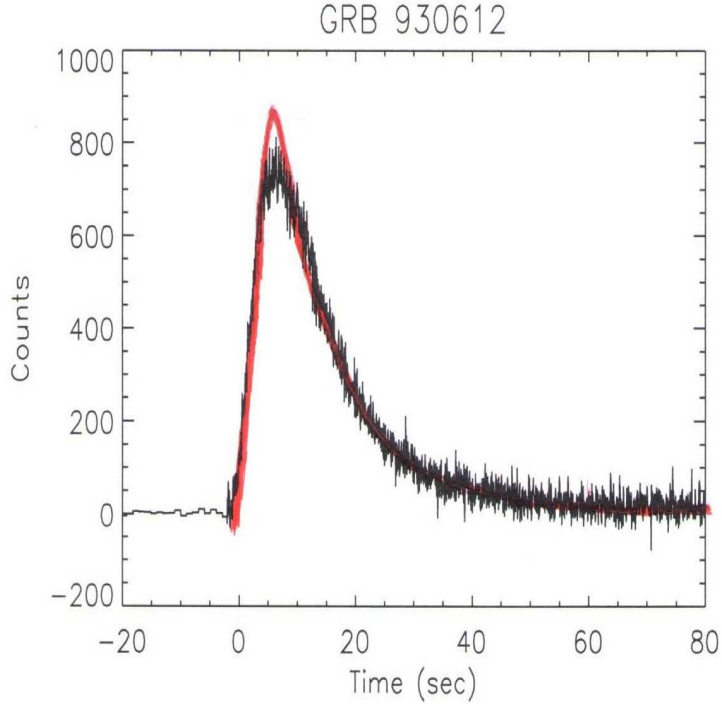


FIG. 6: The pulse shape of GRB930612 measured with BATSE (trigger 2387) aboard CGRO, and the shape given by Eq.(6) for the best fit parameters  $\Delta=6.2$  s and  $\tau=76.3$  s.

Even in the very rare cases where  $\tau/\Delta \approx 1$ ,  $RT/DT \approx 0.57$  and  $RT/FWHM \approx 0.36$ . In Figures 7,8, the CB model predicted ratios  $RT/DT$  and  $RT/FWHM$  for  $\Delta < \tau < \infty$  are compared to their best fit values in 77 resolved pulses of BATSE/CGRO LGRBs reported by Kocevski et al. [43]. As shown in Figures 7,8, their best fit values lie well within the narrow area between the predicted CB model boundaries, and their mean values  $RT/DT = 0.47 \pm 0.08$  and  $RT/FWHMT = 0.31$  reported in [43] are very close to the CB model expected values  $RT/DT = 0.44$  and  $RT/FWHM = 0.31$  for  $\tau = 10 \Delta$ . In Figure 9 we compare the measured pulse shape of SHB170817A and the CB model pulse shape as given in [42] with the best fit parameters  $\Delta = 0.62$  s and  $\tau = 0.57$  s ( $\chi^2/dof = 0.95$ ). The best fit light curve has a maximum at  $t = 0.43$ , a half maximum at  $t = 0.215$  s and  $t = 0.855$  s, with an asymmetry  $RT/DT = 0.50$  and  $RT/FWHM = 0.34$ .

**In the standard fireball models [27]** the GRB prompt emission pulses are produced by synchrotron radiation from shock accelerated electrons in collisions between overtaking thin shells ejected by the central engine or by internal shocks in the ejected conical jet. Only for

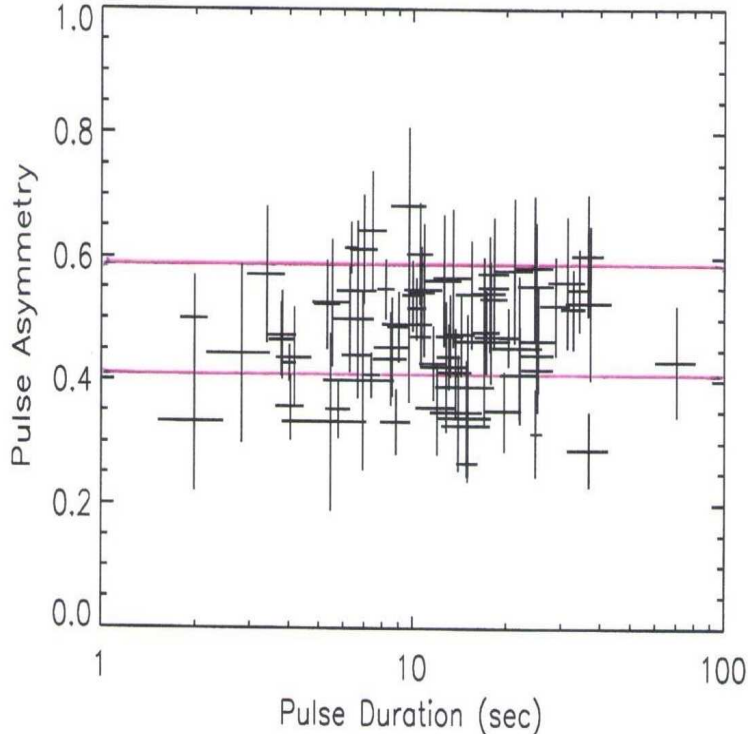


FIG. 7: Comparison between the observed asymmetry ratio  $RT/DT$  as function of pulse duration reported in [43] for a sample of 77 resolved LGRB pulses measured with BATSE aboard CGRO (with a mean value  $RT/DT=0.47\pm 0.08$ ), and the CB model predicted asymmetry  $0.41 < RT/DT < 0.58$  for  $\Delta < \tau < \infty$  (solid lines).

the fast decline phase of the prompt emission, and only in the limit of very thin shells and fast cooling, falsifiable predictions were derived from the underlying FB model assumptions. In this limit the fast decline phase of a pulse was derived from the relativistic curvature effect [39,44,45]. It yields a power law decay

$$F_\nu(t) \propto (t-t_i)^{-(\beta+2)} \nu^{-\beta} \quad (7)$$

where  $F_\nu(t) = E dN/dE$ ,  $t_i$  is the beginning time of the decay phase, and  $\beta$  is the spectral index of prompt emission.

The observed exponential decay of the prompt emission accompanied by a fast spectral softening before the afterglow took over could be roughly reproduced by adjusting a beginning time of the decay and replacing the constant spectral index of the model by the observed time-dependent one [39].

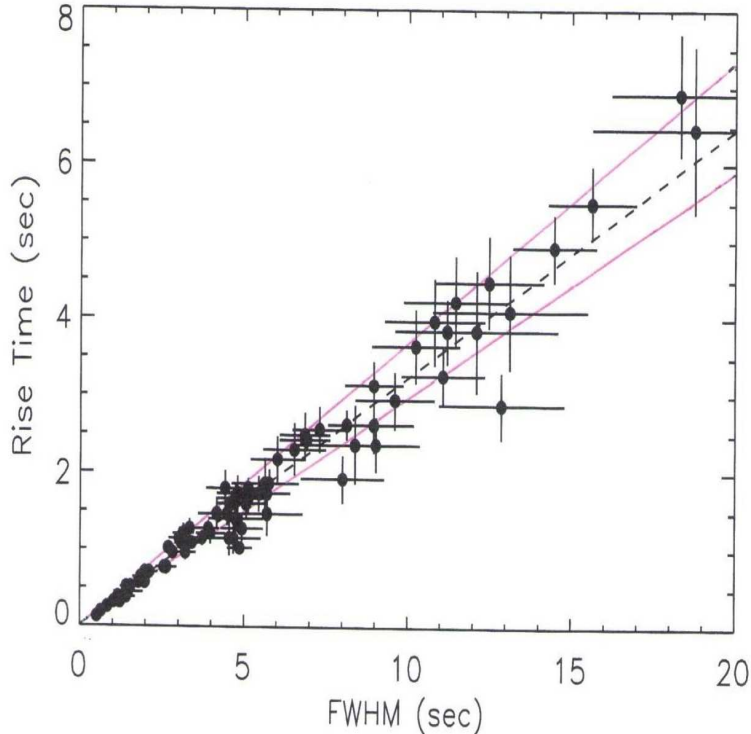


FIG. 8: Comparison between the rise time  $RT$  versus the  $FWHM$  reported in [43] for a sample of 77 resolved pulses measured with BATSE aboard CGRO. The dotted line is best fit ratio  $RT/FWHM = 0.32$  and the solid lines are CB model expected boundaries  $0.29 < RT/FWHM < 0.36$  for LGRBs.

#### IV. AFTERGLOW TESTS

In the **CB model**, the afterglow of SN-GRBs is mainly synchrotron radiation emitted by the highly relativistic jets of CBs launched in core collapse supernova of type Ic (SN-GRBs) in the dense interstellar medium (e.g. molecular clouds where most SNeIc of short lived massive stars take place). The afterglow of SN-less GRBs and ordinary SHBs seems to be dominated by a PWN emission powered by the spin down of a newly born millisecond pulsar [25,26].

In SN-GRBs, the ionized medium in front of the CBs is swept in and generates within them a turbulent magnetic field whose energy density is assumed to be in an approximate equipartition with that of the swept in particles. The electrons that enter the CB with a Lorentz factor  $\gamma(t)$  in the CB's rest frame are Fermi accelerated there and cool by emission of synchrotron radiation (SR), which is isotropic in the CB's rest frame. In the observer

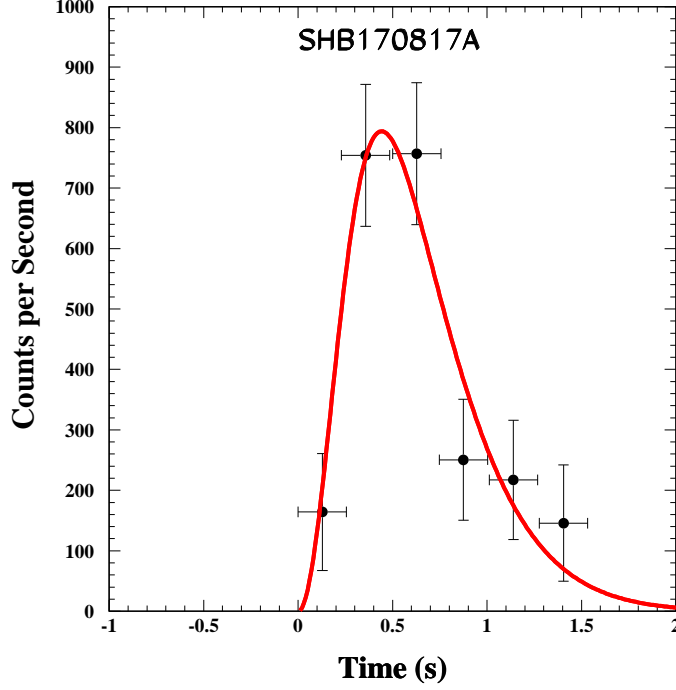


FIG. 9: The pulse shape of SHB170817A measured with the Fermi-GBM [20] and the best fit pulse shape given by Eq.(6) with  $\Delta=0.62$  s and  $\tau=0.57$  s.

frame, the emitted photons are beamed into a narrow cone of an opening angle  $\theta \sim 1/\gamma(t)$  along the CB's direction of motion by its highly relativistic motion, their arrival times are aberrated, and their energies are boosted by its Doppler factor  $\delta$  and redshifted by the cosmic expansion during their travel time to the observer [28].

The observed spectral energy density (SED) flux of the *unabsorbed* synchrotron X-rays,  $F_\nu(t) = \nu dN_\nu/d\nu$ , has the form (see, e.g., Eqs. (28)-(30) in [46]),

$$F_\nu \propto n^{(\beta_x+1)/2} [\gamma(t)]^{3\beta_x-1} [\delta(t)]^{\beta_x+3} \nu^{-\beta_x}, \quad (8)$$

where  $n$  is the baryon density of the external medium encountered by the CB at a time  $t$  and  $\beta_x$  is the spectral index of the emitted X-rays,  $E dn_x/dE \propto E^{-\beta_x}$ .

The swept-in ionized material by the CBs decelerates them. Energy-momentum conservation for such a plastic collision between a CB of a baryon number  $N_B$ , a radius  $R$  and an initial Lorentz factor  $\gamma(0) \gg 1$ , which propagates in a constant density ISM at a redshift  $z$ ,



yields the deceleration law in [42]),

$$\gamma(t) = \frac{\gamma_0}{[\sqrt{(1 + \theta^2 \gamma_0^2)^2 + t/t_d} - \theta^2 \gamma_0^2]^{1/2}}, \quad (9)$$

where  $t$  is the time in the observer frame from the beginning of the afterglow emission by the CBs, and

$$t_d = (1+z) N_B / 8 c n \pi R^2 \gamma_0^3 \quad (10)$$

is its deceleration time-scale.

In the case of SN-less LGRBs, which probably are produced by jets ejected in a phase transition of n\*s to q\*s in high mass X-ray binaries following mass accretion on the n\*s [26], the afterglow appears to be dominated by radiation emitted by the pulsar's wind nebula, powered by the rotational energy loss of the newly born q\* through magnetic dipole radiation, relativistic wind and high energy charged particle emission along open magnetic lines [26].

#### **Test 4: Canonical behavior.**

**In the CB model**, the prompt  $\gamma$ -ray emission was predicted [46] to end with an exponential temporal decay with a fast spectral softening (Eq.6), which is taken over by an X-ray afterglow with a shallow decay phase ("plateau") that breaks smoothly into a power law-decline. This "canonical behavior" [47] was predicted by the CB model (see, e.g., Figures 26-33 in [46]. Figure 31 is shown here as Figure 10) long before the plateau was first observed in the X-ray afterglow of GRB050315 [48] and GRB050319 [49], with the Swift X-ray Telescope (XRT), as shown in Figure 11.

**In the FB model**, no canonical behavior is expected.

#### **Jet Break Tests.**

**In the CB model**, the Lorentz factor  $\gamma(t)$  of a CB, which decelerates in a constant density ISM as given by Eq.(9), change rather slowly as long as  $t < t_b$ , where

$$t_b \approx (1 + \gamma_0^2 \theta^2)^2 t_d. \quad (11)$$

This slow change produces the plateau phase in SN-GRBs. The explicit dependence of  $E_p$  and  $E_{iso}$  on  $\gamma_0$  and  $\delta_0$  can be used to obtain from Eq.(11) the correlation [50],

$$t_b / (1+z) \propto [(1+z) E_p E_{iso}]^{-1/2}, \quad (12)$$

#### **Test 5: Break time correlations.**

The observed break time of the X-ray afterglow of SN-LGRBs measured with the Swift

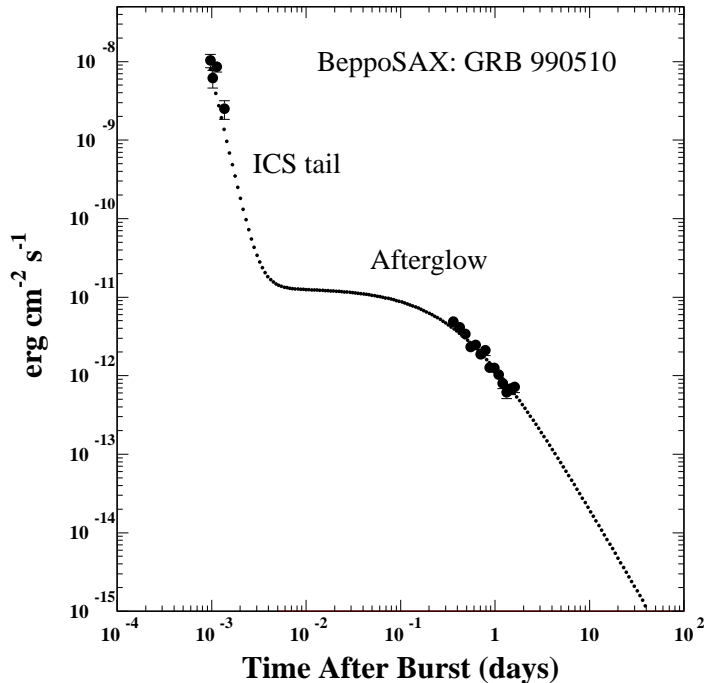


FIG. 10: The X-ray afterglow of GRB 990510 measured with the telescopes aboard the BeppoSAX satellite compared to a canonical X-ray afterglow predicted by the CB model [46] for SN-GRBs.

XRT [51], for SN-LGRBs with known redshift,  $E_p$  and  $E_{iso}$ , is compared in Figure 12 to that predicted by Eq.(12). As shown in Figure 12, it is well satisfied by such SN-GRBs.

### Test 6: Post break closure relations.

Far beyond the break, Eq.(9) yields  $\delta(t) \approx 2\gamma(t) \propto t^{-1/4}$  [50]. When substituted in Eq.(8), it yields the late-time behavior,

$$F_\nu(t \gg t_b) \propto t^{-\alpha_\nu} E^{-\beta_\nu}, \quad (13)$$

which satisfies the closure relation

$$\alpha_\nu = \beta_\nu + 1/2. \quad (14)$$

This post break closure relation is well satisfied by the X-ray afterglow of SN-GRBs [50] as long as the CB moves within roughly a constant density interstellar medium. It is demonstrated in Figure 13 for the X-ray afterglow of GRB060729 [51], a canonical afterglow of an SN-GRB. Its long followed up and well sampled X-ray afterglow yielded a best fit temporal index  $\alpha_x = 1.46 \pm 0.03$ , which agrees well with  $\alpha_x = \beta_x + 1/2 = 1.49 \pm 0.07$  for an observed [51]  $\beta_x = 0.99 \pm 0.07$ . The most accurate test, however, of the CB model relation

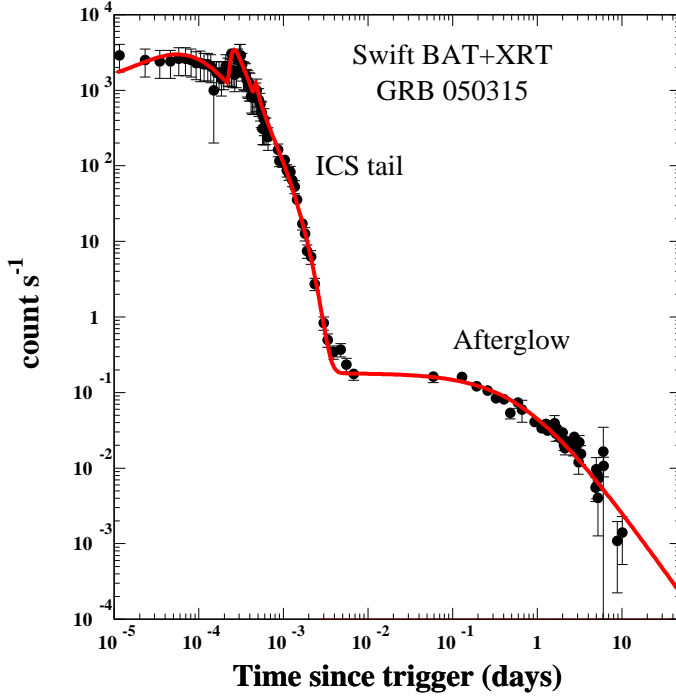


FIG. 11: The X-ray afterglow of GRB050315 measured with the telescopes aboard Swift compared to its best fit canonical X-ray afterglow predicted by the CB model [46] for SN-GRBs.

$\alpha_x = \beta_x + 1/2$  for a single SN-GRB was provided by the follow-up measurements of the X-ray afterglow of GRB 130427A, the most intense GRB ever detected by Swift and followed with the Swift XRT and other sensitive X-ray telescopes aboard XMM Newton and CXO up to a record time of 83 Ms after burst [52]. The measured light-curve has a single power-law decline with  $\alpha_x = 1.309 \pm 0.007$  in the time interval 47 ks - 83 Ms. The best single power-law fit to the combined measurements of the X-ray light-curve of GRB 130427A with the Swift-XRT [17], XMM Newton, CXO [52], and MAXI [53] that is shown in Figure 14 yields  $\alpha_x = 1.294 \pm 0.03$ . The CB model prediction as given by Eq.(14) with the measured spectral index  $\beta_x = 0.79 \pm 0.03$  [52], is  $\alpha_x = 1.29 \pm 0.03$ , in remarkable agreement with its best fit value. No doubt, the assumptions of a constant density circumburst medium is an over simplification: SN-LGRBs that are produced by supernova explosions of type Ic or short-lived massive stars, take place mostly in superbubbles formed by star formation. Such superbubble environments may have a bumpy density, which deviates significantly from the assumed constant-density ISM. It may be responsible for the observed deviations from the

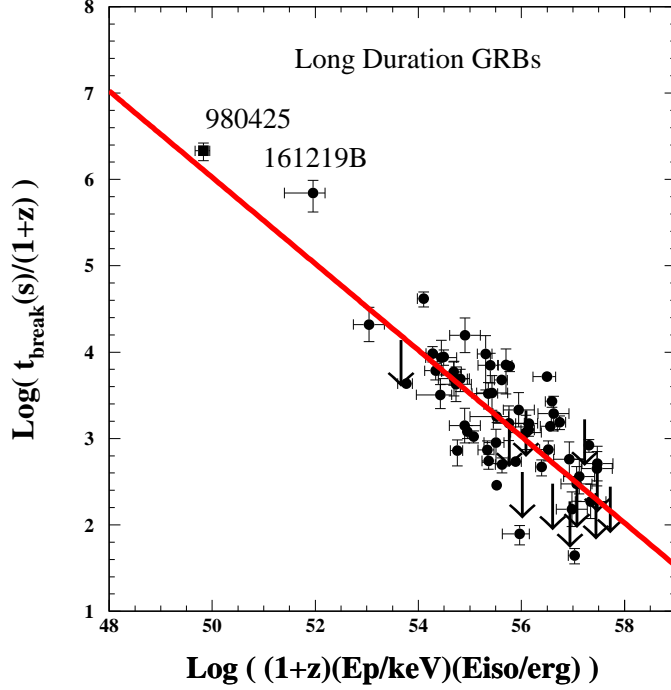


FIG. 12: The break time  $t_b/(1+z)$  of the X-ray afterglow of LGRBs measured with the Swift XRT [51], as a function of  $[(1+z) Ep Eiso]$ . The line is the CB model correlation given by Eq.(12), which is expected in SN-GRBs. SN-Less GRBs that are identified by an afterglow with a light curve  $\propto 1/(1+t/t_b)^2$  [26] are not included.

predicted smooth light-curves and for  $\chi^2/dof$  values slightly larger than 1. Moreover, in a constant-density ISM, the late-time distance of a CB from its launch site is given roughly by,

$$x = \frac{2c \int^t \gamma \delta dt}{1+z} \approx \frac{4c \gamma_0^2 \sqrt{t_b t_d}}{1+z}. \quad (15)$$

This distance can exceed the size of the superbubble and even the scale-height of the disk of the GRB host galaxy. In such cases, the transition of a CB from the superbubble into the Galactic ISM or into the Galactic halo, in face-on disk galaxies, will bend the late-time single power-law decline into a more rapid decline, depending on the density profile above the disk. For instance, when the CB exits the disk into the halo, its Lorentz and Doppler factors tend to constant values while its afterglow decays roughly like ((see Eq.(8))

$$F_\nu(t) \propto [n(r)]^{(1+\beta_\nu)/2} \quad (16)$$

where  $r \propto t$ . Such a behavior may have been observed by the Swift XRT [51] in several

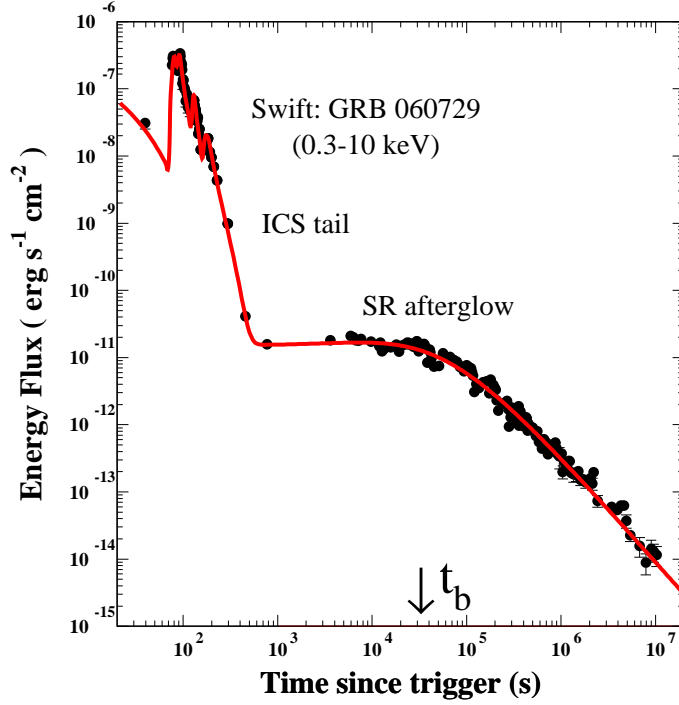


FIG. 13: The canonical light curve of the X-ray afterglow of the SN-GRB 060729 measured with Swift XRT [51], and its best fit CB model afterglow [28] as given by Eq.(8) which well satisfies the CB model prediction  $\alpha_x = \beta_x + 1/2$ .

GRBs, such as 080319B and 110918A, at  $t > 3 \times 10^6$  s and in GRB 060729 at  $t > 3 \times 10^7$  s by CXO [54].

### Test 7: Missing breaks.

**In the CB model**, Eq.(8) yields a single power-law for the temporal decline of the light curve of the afterglow well beyond the break time  $t_b$  as long as the CB moves in a constant density interstellar medium. Consequently, in the CB model, very energetic LGRBs, i.e., those with a large product  $(1+z)E_p E_{iso}$ , may have a break time  $t_b$  smaller than the time when the afterglow takes over the prompt emission, or before the afterglow observations began [55]. In such cases the observed afterglow light curve has a single power-law behavior with a temporal decay index  $\alpha_\nu = \beta_\nu + 1/2$  and a "missing break". This was first observed in GRB 061007 [56], with the Swift XRT [51] as demonstrated in Figure 15. The  $\alpha_x$  values of the most energetic LGRBs with known redshift that were obtained from the Swift XRT measurements are plotted in Figure 16 as function of their measured  $\beta_x + 1/2$  values. Also

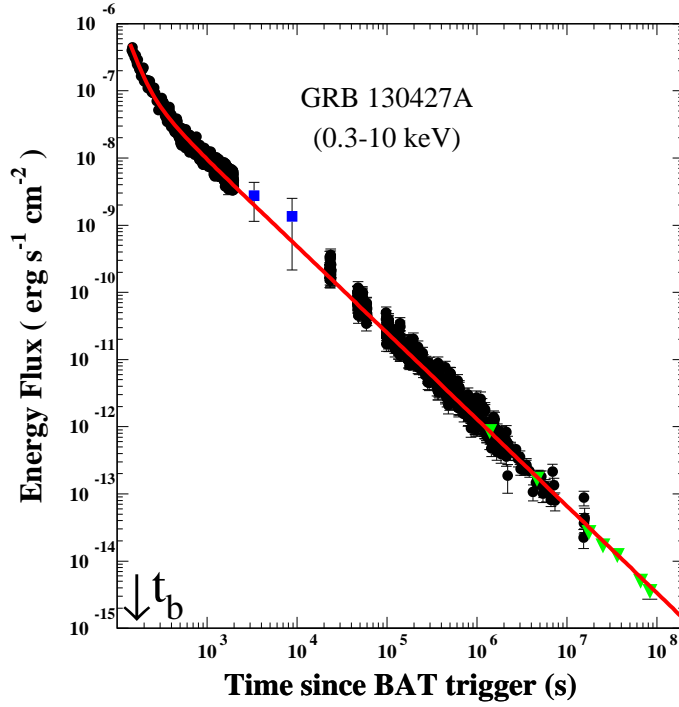


FIG. 14: The X-ray light-curve of the intense GRB 130427A that was measured with Swift XRT [51] (circles) and with XMM Newton and Chandra [52] (triangles) up to 83 Ms after burst, and its CB model best-fit with a start time and an early break hidden under the prompt emission phase. Also shown are the two MAXI data points [53] (squares) at  $t = 3257$  s and  $t = 8821$  s. The best-fit power-law decline has an index  $\alpha_x = 1.29$ . The temporal decay index predicted by the CB model, Eq.(14), for the measured spectral index [52]  $\beta_x = 0.79 \pm 0.03$  is  $\alpha_x = 1.29 \pm 0.03$ .

plotted is the best fit linear relation  $\alpha_x = a(\beta_x + 1/2)$ , which yields  $a=1.007$ , in good agreement with  $a=1$  predicted by the CB model.

**In the FB models**, the existence of a GRB afterglow at longer wave lengths was predicted [12] long before it was discovered in the X-ray band by the telescopes aboard the Beppo-SAX satellite [13] and then by ground based optical and radio telescopes [14]. In the first two years after their discovery, the observed light curves of these afterglows were claimed to be well fitted by a single power-law [58], predicted for spherical fireballs [59],[60]. Later when the observations clearly indicated a smoothly broken power-law behavior rather than a single power-law, the spherical  $e^+e^-\gamma$  fireball have been replaced without much ceremony, first with conical flows or a succession of thin conical shells of  $e^+e^-\gamma$  plasma, and later by

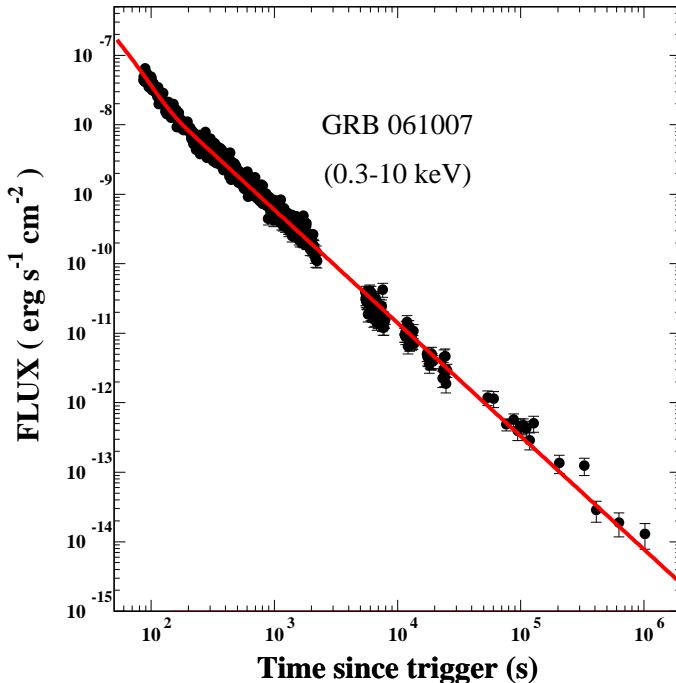


FIG. 15: The single power-law best fit to the afterglow of GRB061007 with a "missing jet break" measured with Swift XRT [56]. The best fit temporal index  $\alpha_x = 1.65 \pm 0.01$  satisfies the CB model prediction  $\alpha_x = \beta_x + 1/2 = 1.60 \pm 0.11$ .

plasma of ordinary matter. These flows retained the name "collimated fireballs" and the revised models retained the "fireball model" name. However, these collimated fireballs could neither explain, nor reproduce correctly the observed behavior of the afterglow of SN-GRBs and failed tests 4-7:

**Test 4 (Canonical behavior):** The afterglows were predicted to decay like a broken power-law [61], but could not explain/reproduce the 'plateau phase' of the afterglow observed in many GRBs without postulating a continued energization [62] of the jet by the central engine.

**Test 5 (Break time correlation):** In the standard fireball models, the opening angle of the conical jet satisfies  $\theta_j \gg 1/\gamma_0$ . Because of relativistic beaming, initially only a fraction  $\sim 1/\gamma^2 \theta_j^2$  of the front surface of the jet is visible to a near axis, distant observer. This fraction, increases with time like  $[\gamma(t)]^{-2}$ , due to the deceleration of the jet in the interstellar medium (ISM), until the entire front surface of the jet becomes visible, i.e., until  $t \approx t_b$  where

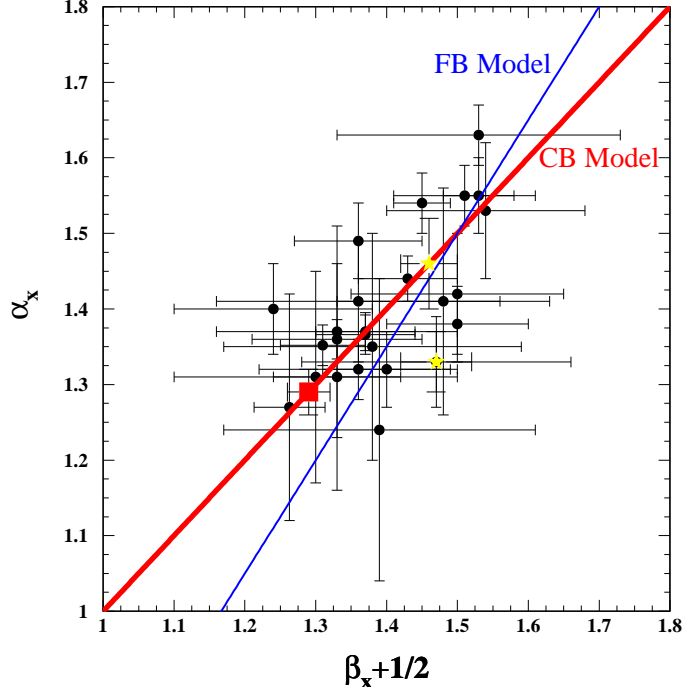


FIG. 16: The values of the post break temporal index  $\alpha_x$  as function of the spectral index  $\beta_x + 1/2$  for the 28 most intense GRBs with known redshift [57] that were obtained from the follow-up measurements of their 0.3-10 keV X-ray afterglow with the Swift XRT [51]. The square indicates the value obtained for GRB 130427A. The thick line is the CB model prediction, Eq.(14).

$\gamma(t_b) = 1/\theta_j$ . If the total  $\gamma$ -ray energy  $E_\gamma$  is assumed to be a constant fraction  $\eta$  of the initial kinetic energy  $E_k$  of the jet, which decelerates in an ISM of a constant baryon density  $n_b$  by sweeping in (*plastic collision*) the interstellar matter on its trajectory, then [63]

$$t_b/(1+z) \approx \frac{1}{16c} \left[ \frac{3E_{iso}}{\eta\pi n_b m_p c^2} \right]^{1/3} [\theta_j]^{8/3}. \quad (17)$$

Although the standard fireball model assumes that the afterglow is synchrotron radiation emitted by the shocked ISM (i.e., through *elastic scattering* of the ISM particles in front of the jet, and not by *plastic collision*, see Table II), Eq.(17) has been used widely in the literature to estimate  $\theta_j$  without any justification..

Moreover, if  $E_\gamma \approx \eta E_k \approx E_{iso}\theta_j^2/4$  is a "standard candle" [64], then  $E_{iso}\theta_j^2 \approx const$  and

$$t_b/(1+z) \propto [E_{iso}]^{-1}. \quad (18)$$

The same  $[t_b, E_{iso}]$  correlation is obtained for the deceleration of a conical jet in a wind-like



TABLE II: The late time  $t$ -dependence of the bulk motion Lorentz factor of highly relativistic conical jets which decelerate by collision with the surrounding medium.

Collision:	Plastic	Plastic	Elastic	Elastic
Density:	ISM	Wind	ISM	Wind
$\gamma(t) \propto$	$t^{-3/8}$	$t^{-1/4}$	$t^{-3/7}$	$t^{-1/3}$

circumburst density [65]. However, Eq.(18), the expected  $[t_b, E_{iso}]$  correlation in the FB model, was shown [66] to be inconsistent with the best fit correlation  $t_b/(1+z) \propto E_{iso}^{-0.69 \pm 0.06}$  to the observational data. The observational data, however, is consistent with the correlation  $t_b/(1+z) \propto E_{iso}^{-0.75}$  expected in the CB model [66].

**Test 6: Closure relations.** In the conical fireball model, the increase of the visible area of the conical jet with time like  $1/[\gamma(t)]^2$  that stops at  $t_b$  yields an achromatic temporal break in the GRB afterglow. If the afterglow is parametrized as  $F_\nu(t) \propto t^{-\alpha} \nu^{-\beta}$ , the predicted change in  $\alpha$  across the break is achromatic and satisfies

$$\Delta(\alpha) = \alpha(t > t_b) - \alpha(t < t_b) = 3/4 \quad (19)$$

for a constant ISM density. For a wind like density,  $\Delta(\alpha) = 1/2$ . This closure relation for either an ISM or a wind like density is not satisfied by most GRB breaks, as can also be seen in Figures 10-15. In fact, Liang, et al. [67] analyzed the afterglow of 179 GRBs detected by Swift between January 2005 and January 2007 and the optical AG of 57 pre-Swift GRBs. They did not find any afterglow with a break satisfying tests 5,6.

**Test 7 (Missing breaks):** The missing break in the X-ray afterglow of several GRBs with a long follow up measurements was suggested to take place after the observations ended [68]. But, Eq.(18) implies that late-time breaks are present only in GRBs with a small  $E_{iso}$ . This, suggestion is in contradiction with the fact that missing breaks in GRBs with well sampled afterglows, which extend to late times, are limited to GRBs with very large  $E_{iso}$ , rather than small  $E_{iso}$ . This is demonstrated in Figures 15,14 by the unbroken power-law X-ray afterglows of GRBs 061007 and 130427A, where  $E_{iso} = 1E54$  erg [56] and  $E_{iso} = 8.5E53$  erg [52], respectively, which satisfy well the CB model post break closure relation given by Eq.(14)

### Test 8: Chromatic Jet Breaks

**In the CB model** the jet deceleration break in the afterglow of jetted SN-GRBs is dynamic in origin and usually chromatic [28].

**In the FB model** the jet breaks in the afterglows of jetted SN-GRBs are basically geometrical in origin and therefore are predicted to be mostly achromatic [27], in conflict with observations.

### Test 9: Universal afterglow of SN-less GRBs.

Figure 17, adapted from [69] shows the X-ray light curve of GRB 990510 measured with BeppoSAX, whose afterglow could not be fit well by a single power-law predicted by spherical fireball models (e.g., [69]). It could, however, be fit well by an achromatic "smoothly broken power law" parametrizations [69] as shown in Figure 18. That, and the observed optical and X-ray afterglows of a couple of other GRBs detected by BeppoSAX, which could be fit by a smoothly broken power-law, led to the replacement of the spherical  $e^+e^-\gamma$  fireball by an  $e^+e^-\gamma$  "conical fireball" which was later replaced with a conical jet of ordinary matter and became the current standard collimated fireball model of GRBs. But, the afterglow of GRB 990510 and other GRBs which were fit by smoothly broken single power laws are not conclusive evidence of being produced by a conical jets. In fact, an isotropic radiation from a pulsar wind nebula powered by a newly born millisecond pulsar has an expected luminosity [26] which satisfies

$$L(t) = L(0)/(1+t/t_b)^2 \quad (20)$$

where  $t_b = P(0)/2\dot{P}(0)$ , and  $P(0)$  and  $\dot{P}(0)$  are, respectively, the initial period and its time derivative, of the newly born pulsar. This is shown in Figure 18 for GRB 990510. In particular, if the afterglows of SN-less GRBs are produced by PWNs powered by the newly born MSPs, then  $L(t)/L(0)$  has a *universal temporal behavior* [22] as a function of  $t/t_b$ ,

$$L(t/t_b)/L(0) = 1/(1+t/t_b)^2 \quad (21)$$

This *universal behavior* describes well the X-ray and optical afterglow light curves of GRB 990510, as shown in Figures 18,19. It also describes well the afterglow of all SN-less GRBs and SHBs with a well sampled afterglow within the first couple of days after burst. This is demonstrated in Figure 20 for the X-ray afterglow of 12 SN-less GRBs, and in Figure 21 for all the 12 SHBs [22] from the Swift XRT light curve repository [51] with a well sampled afterglow during the first few days after burst.

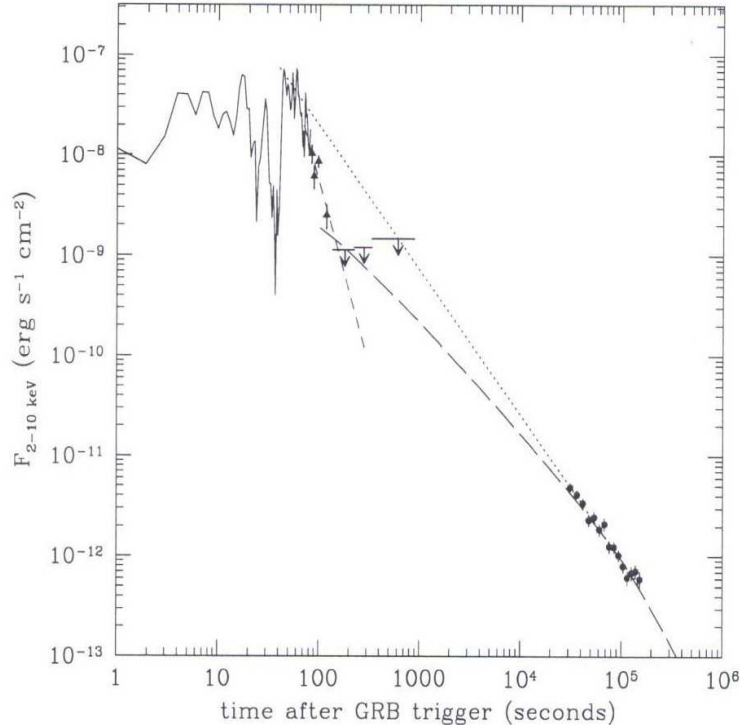


FIG. 17: The X-ray light curve of GRB 990510 and its afterglow measured with BeppoSAX together with a single power-law fit and a smoothly broken single power-law fit to its X-ray afterglow [69].

## V. PROGENITORS OF LONG GRBS

### Test 10: Redshift Distribution of long GRBs.

**In the CB model** long duration GRBs belong to two classes, SN-GRBs that are produced in stripped envelope supernovae of type Ic (SNeIc) and SN-less GRBs that presumably are produced in a phase transition of neutron stars to quark stars following mass accretion in high mass X-ray binaries [11,22]. In both cases, the progenitors involve a short lived high mass star. Hence, in the CB model, the observed production rate of long GRBs is proportional to the star formation rate [72] modified by beaming [73].

Figure 22 compares the observed distribution of long GRBs as a function of redshift and their expected distribution in the CB model assuming their production rate is proportional to the SFR modified by beaming [73]). **In the FB models** where  $\theta_j \gg 1/\gamma(0)$  the observed rate of GRBs is expected to be proportional to the star formation rate (SFR) [72] back to very large redshifts beyond those accessible to optical measurements. However, the observed rates

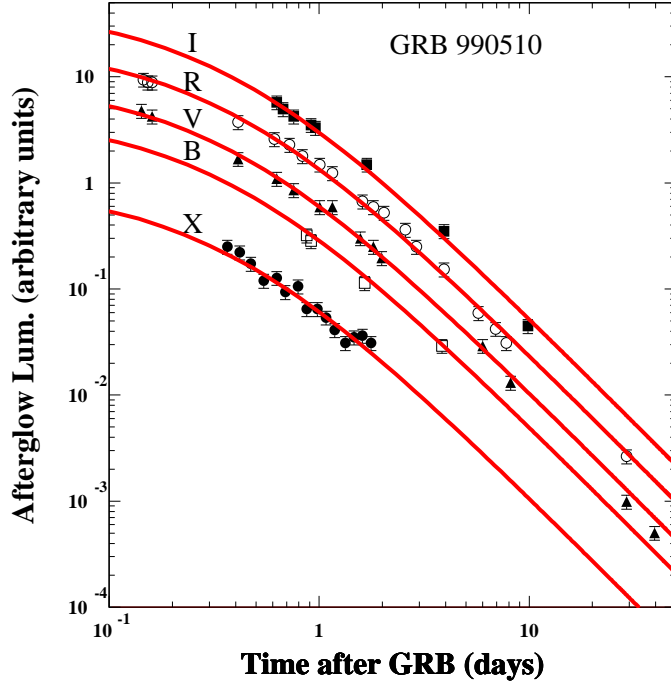


FIG. 18: Comparison of Eq.(20), the predicted temporal behavior of the light curves of the X-ray and optical afterglows of GRB990510 and their observed light curves. The X-ray data at 5 keV (filled circles) is from [69]. The data in the bands I (filled squares), R (empty circles), V (filled triangles) and B (open squares) are that compiled in [69] from [70]. The flux normalization is in arbitrary units.

of LGRBs and XRFs do not follow the SFR. Unlike the SFR (in a comoving unit volume), which first increases with redshift, [73] the observed rate of LGRBs first decreases with increasing redshift in the range  $z \leq 0.1$ , even after correcting for detector flux threshold [74]. At larger redshifts, it increases faster than the SFR [75]. The discrepancy at small  $z$  was interpreted as evidence that ordinary LGRBs and low-luminosity LGRBs and XRFs with much lower luminosity belong to physically distinct classes [76]. The discrepancy at  $z \gg 1$  was claimed to be due to different evolutions [77]. Figure 23, also displays the cumulative distribution of GRBs as function of redshift in the standard fireball model, with the redshift evolution of the LGRBs relative to the SFR assumed in [77]. As can be seen from Figure 23, the observational data does not support the evolution proposed in [77].

### Test 11: Low Luminosity GRBs.

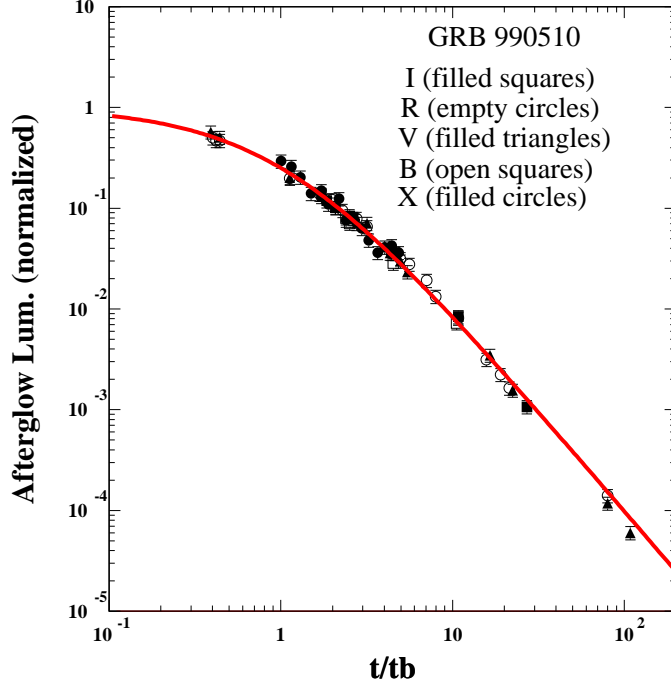


FIG. 19: Comparison between the normalized light curves of the X-ray and optical afterglows of GRB990510 and their predicted universal shape as given by Eq.(21). Data is the same as in Figure 18.

**In the CB model** the observed properties of GRBs depend strongly on their viewing angle relative to the CBs' direction of motion. Ordinary (OR) GRBs are viewed from angles  $\theta \sim 1/\gamma_0$  relative to the CB direction of motion, which yield  $\delta_0 \sim \gamma$ . In the CB model, low luminosity (LL) GRBs are ordinary GRBs with similar intrinsic properties, but viewed from far off-axis, i.e.,  $\gamma_0 \delta_0 = (1 - \beta \cos \theta) \approx 2/\theta^2$ . Consequently, under the approximation that GRBs are standard candles, ordinary GRBs and LL GRBs satisfy the relations

$$E_{iso}(LL \text{ GRB}) \approx E_{iso}(OR \text{ GRB})/[\gamma_0^2 (1 - \cos \theta)]^3 \quad (22)$$

$$L_p(LL \text{ GRB}) \approx L_p(OR \text{ GRB})/[\gamma_0^2/(1 - \cos \theta)]^4 \quad (23)$$

. Eqs.(22),(23) and the predicted correlations between properties of LL GRBs can be used to test the far off-axis ( $[\gamma(0)\theta]^2 \gg 1$ ) identity of LL-GRBs. These correlations include:

a)  $(1+z)E_p \propto E_{iso}^{1/3}$ , which is verified in Figure 4.

b)  $(1+z)t_b \propto [(1+z)E_p E_{iso}]^{-1/2}$ ,

valid for both near axis and far off-axis SN-GRBs, which is verified in Figure 12.

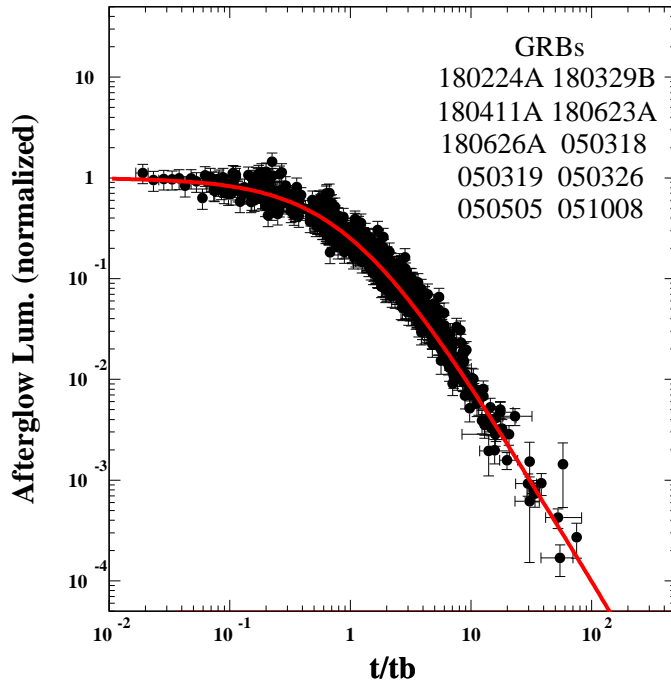


FIG. 20: Comparison between the normalized light curve of the X-ray afterglow measured with Swift XRT [51] of 12 SN-less GRBs with a well sampled afterglow in the first couple of days after burst and their predicted universal behavior as given by Eq.(21).

c) Production rate per comoving unit volume which is proportional to the star formation rate with the same proportionality constant as that for ordinary GRBs, after correcting for viewing angle, which is verified in [73] and in Figure 23.

Perhaps, the best evidences that both low-luminosity and ordinary SN-GRBs belong to the same class of GRBs comes from the fact that both types of SN-GRBs are produced in very similar SNeIc [23] akin to SN1998bw. For instance, SN2013cq that produced GRB130427A at redshift  $z=0.34$ , with a record high GRB fluence measured by Swift BAT and Fermi GBM, and with an  $E_{iso} \sim 10^{54}$  erg, was very similar [23] to SN1998bw, which produced the LL GRB980425 with a record low  $E_{iso} \sim 10^{48}$  erg [78], roughly smaller by a factor  $10^6$ .

Moreover, the best fit CB model light curve of the X-ray afterglow of GRB980425

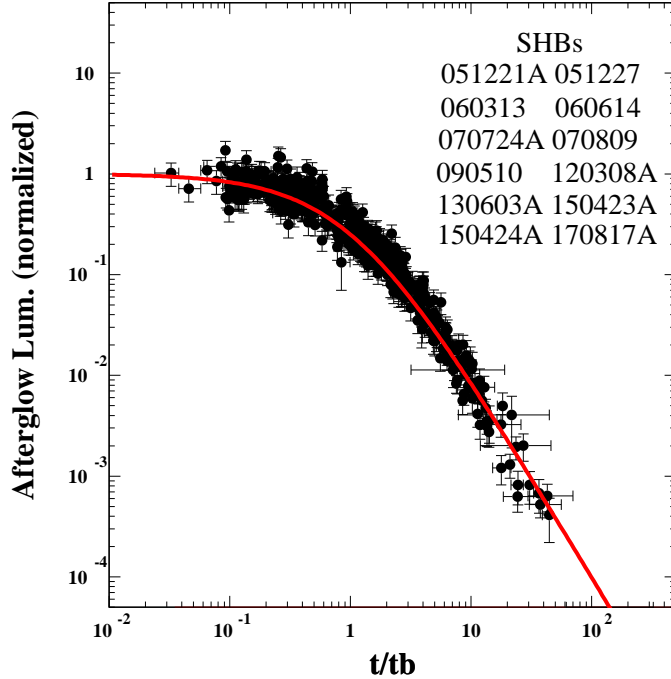


FIG. 21: Comparison between the normalized light curve of the X-ray afterglow of 11 SHBs with a well sampled afterglow measured with the Swift XRT [51] during the first couple of days after burst and the predicted universal behavior given by Eq.(21). The bolometric light curve of SHB170817A reported in [71], is also included.

measured with Beppo-SAX [79] and CXO [80] shown in Figure 24, has yielded  $\gamma\theta \approx 8.7$ . Thus, Eq.(22) yields  $E_{iso}(GRB980425) \approx 1.84 \times 10^{-5} \langle E_{iso}(OR GRB) \rangle \approx 1.3 \times 10^{48}$  erg for  $\langle E_{iso}(OR GRB) \rangle \approx 7 \times 10^{52}$  erg in good agreement with the observed value [78]  $E_{iso}(GRB980425) \approx (1 \pm 0.2) \times 10^{48}$  erg.

**In the FB model**, low luminosity GRBs were claimed to be intrinsically different from ordinary SN-GRBs and belong to a different class [76] of GRBs. This has been forced upon the fireball model because of three reasons:

- a) The standard fireball model could not explain  $\sim 6$  orders of magnitudes difference between the value of  $E_{iso}$  of low luminosity SN-GRBs, such as that of GRB980425, and that of very high luminosity SN-GRBs, such as GRB130427A, which were produced by very similar SNeIc [23].

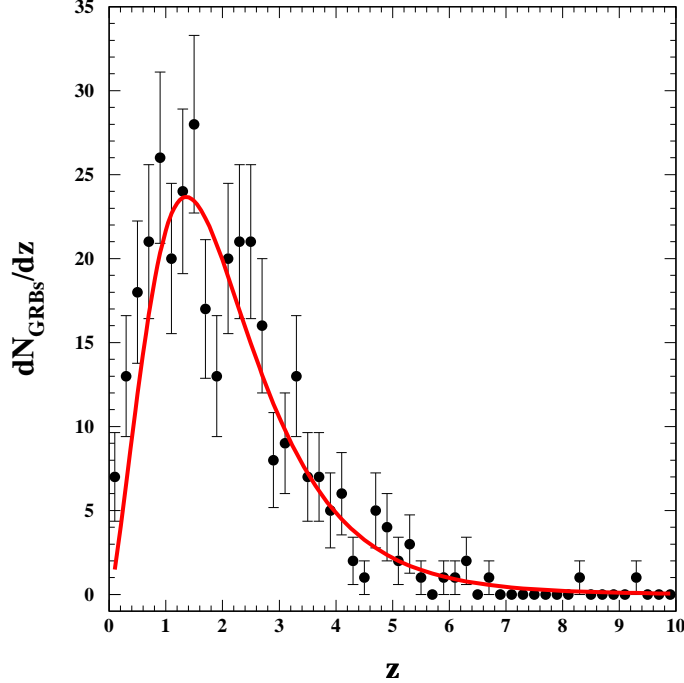


FIG. 22: Comparison between the redshift distribution of 356 long GRBs with known redshift observed before June 2018 and their expected distribution in the CB model if the production rate of GRBs is proportional to the SFR; ( $\chi^2/dof = 37.57/49 = 0.77$ ).

- b) The SN-GRB association and the observed locations of long GRBs in star formation regions of galaxies suggested [72] that long GRBs trace the star formation rate. However, it was found that the redshift distribution of LGRBs at  $z < 0.1$  does not follow the SFR [77]: while the SFR in a comoving unit volume first increases with redshift, the observed rate of long GRBs in the range  $z < 0.1$  decreases with increasing redshift.
- c) The observed production rate of low luminosity GRBs at  $z < 0.1$  relative to the SFR is larger by a large factor than the ratio at much higher  $z$  values [77]).

Note, however, that despite the past widespread belief among the FB models promoters that LL-GRBs and OR-GRBs belong to two distinct classes of long GRBs [76], the far off-axis jet origin of the low luminosity SHB170817A, has now been widely accepted. This followed its measured  $E_{iso} \approx (5.4 \pm 1.3) \times 10^{46}$  erg [81], which was smaller by roughly five orders of magnitudes than that of ordinary SHBs, and from the measured viewing angle by Ligo-Virgo, of the axis of the n\*n\* binary which produced GW170817 [21], from the



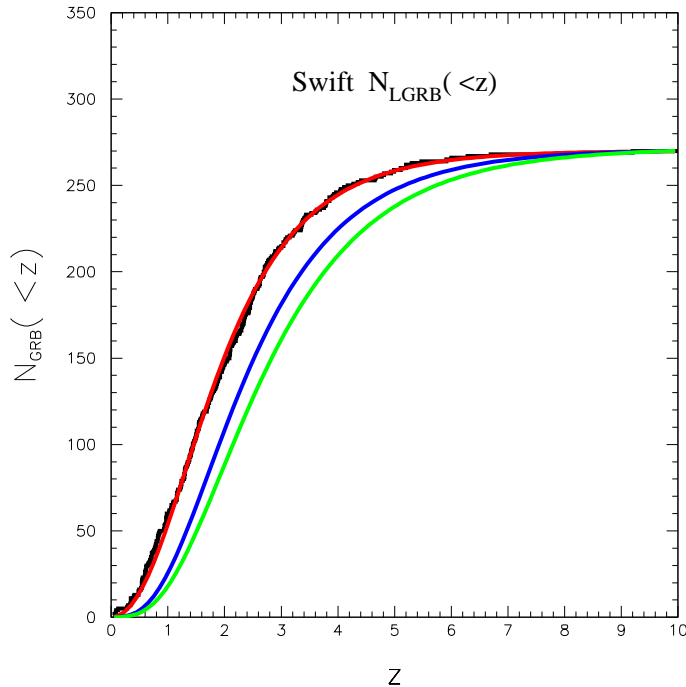


FIG. 23: Comparison between the cumulative distribution function,  $N(< z)$ , of the 262 LGRBs with known redshift (histogram) that were detected by Swift before 2014 and  $N(< z)$  expected in the CB model (left curve) for long GRBs whose rate traces the SFR. Also shown is the distributions expected in FB models with evolution (left and right curves) [77] and without evolution (middle curve).

observed behavior of its late time afterglow [82], and from the measured superluminal motion of its point-like radio source [83](see Tests 12, 13).

Test 12: Superluminal Velocity in SN-GRBs. The first observation of an apparent superluminal velocity of a source in the plane of the sky was reported [84] in 1902, and since 1977 in many high resolution observations of highly relativistic jets launched by quasars, blazars, and microquasars. The correct interpretation of such observations within the framework of special relativity was provided in [85].

A relativistic source with a velocity  $\beta c$  at redshift  $z$  which is viewed from an angle  $\theta$  relative to its direction of motion and is timed by the local arrival times of its emitted

photons, has an apparent velocity in the plane of the sky, which is given by,

$$V_{app} = \frac{\beta c \sin\theta}{(1+z)(1-\beta \cos\theta)} = \frac{\beta \gamma \delta c \sin\theta}{(1+z)}. \quad (24)$$

For  $\gamma \gg 1$ ,  $V_{app}$  has a maximum value  $\approx 2\gamma c/(1+z)$  at  $\sin\theta = 1/\gamma$ .

The predicted superluminal velocity of the jetted CBs, which produce GRBs cannot be verified during the prompt emission phase, mainly because of its short duration and the large cosmological distances of GRBs. However, the superluminal velocity of the jet in far off-axis, i.e., nearby low luminosity GRBs, can be obtained from high resolution follow up measurements of their afterglows [86]. Below, we discuss two cases.

**a. GRB980425.** So far, the radio and X-ray afterglow of GRB980425, the nearest observed SN-GRB with a known redshift,  $z=0.0085$ , has offered the best opportunity to look for the superluminal signature of the highly relativistic jets, which produce GRBs [86]. To the best of our knowledge, this has been totally overlooked in the late-time high resolution X-ray [80] and radio observations [87] of SN1998bw/GRB980425 due to biases. But if these transient sources observed on day 1281 and 2049.19, respectively, in the same direction from SN1998bw, are the CB which produced GRB980425, then it moved with an apparent superluminal jet velocity of  $V_{app} \approx 340 c$  and a viewing angle  $\theta \approx 2 c/V_{\perp} \approx 1/170$  rad [85]. This interpretation implies that these sources are not present there anymore, and were not there before SN1998bw/GRB980425.

Supportive evidence for this CB model value of  $V_{app}$  in GRB980425 is provided by other observations.

(i) The expected value  $E_p \approx \epsilon_p \gamma \delta / (1+z) \approx 1 eV / 1.0085 (1 - \cos\theta) \approx 57$  keV, which is in good agreement with the observed [78] value  $E_p = 55 \pm 21$  keV.

(ii) The ratio of the observed  $FWHM \approx R_g \theta^2 / c \approx 12$  s duration of GRB980425 and the observed mean  $FWHM \approx \langle 2(1+z) R_g / \gamma^2 c \rangle = 0.89$  s duration of ordinary GRBs [87] yield  $\gamma \theta \approx 9$  for the observed average  $\langle 1+z \rangle \approx 3$ . Thus, Eq.(21) yields  $E_{iso}(GRB980425) \approx 1.1 \times 10^{48}$  erg, in good agreement with its measured value [78]  $E_{iso}(GRB980425) \approx (1.0 \pm 0.2) \times 10^{48}$  erg.

(iii) The 0.3-10 keV X-ray light-curve of the afterglow of GRB980425 measured by BeppoSAX [79] and CXO [80] can be well fit by the CB model with  $\gamma \theta \approx 8.7$  as shown in Figure 24.

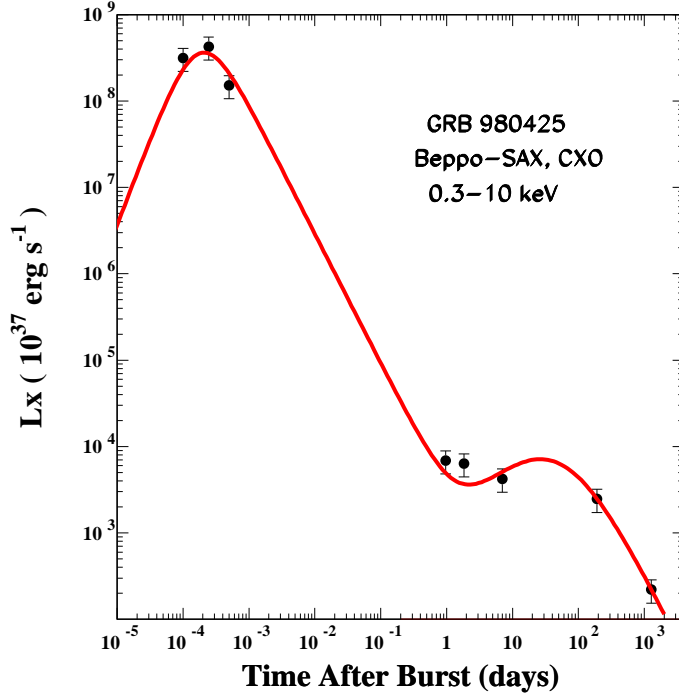


FIG. 24: The 0.3-10 keV X-ray light-curve of GRB980425 measured by Beppo-SAX [79] (first 7 points). The last point at 1281 days is due to the source S1b resolved by CXO [80]. The line is the CB model best fit light-curve to the prompt emission pulse and the afterglow of GRB980425 for  $\gamma\theta \approx 8.7$ .

**b. GRB030329.** The relative proximity ( $z=0.1685$ ) of GRB030329 and its record-bright radio afterglow made possible its record long, high resolution follow-up observations with the Very Long Baseline Array (VLBA) and Very Long Baseline Interferometry (VLBI), until 3018.2 days post GRB [88]. Assuming a disk shape, the radio image of GRB030329/SN2003dh was fit with a circular Gaussian of diameter  $2R_{\perp}(t)$ . The mean apparent image expansion, before time  $t$ , is

$$\langle \beta_{app} \rangle = 2R_{\perp}/ct. \quad (25)$$

SN2003dh and GRB030329, however, had individual image sizes much smaller than the resolution of the VLBA and VLBI arrays: The initial large expansion velocity of broad-line SNeIc, such as SN2003dh decreases to less than 10,000 km/s within the first month, beyond which it continues to decrease, roughly like  $t^{-1/2}$ . Such an expansion velocity yields SN image-sizes  $< 0.002$  pc and  $< 0.005$  pc on days 25 and 83 after burst, compared to the

joint image-size of GRB030329/SN2003dh,  $\sim 0.2$  pc and  $\sim 0.5$  pc, respectively, extracted from the radio observations [88]. As for CBs, time dilation and ram pressure suppress their lateral expansion in the circumburst medium, as long as they move with a highly relativistic speed. Although their small size implies radio scintillations, the large time-aberration wash them out by the time-integrated measurements in the observer frame – the typical  $dt \sim 100$  minutes integration time of the VLBA observations [88] corresponds to an early effective image size  $V_{perp} dt \geq 10^{16}$  cm.

The VLBA and VLBI measurements [89] could not resolve the separate images of SN2003dh and the CB, which produced GRB030329 and its afterglow, nor the superluminal displacement the CB away from SN2003dh. If, however, the size of their joint radio image and its expansion rate as measured in [89] are adapted as a rough estimate of the time-dependent distance between the GRB afterglow and the SN, they can be used to test the CB model, as shown below.

In ordinary GRBs, CB deceleration in an ISM with a constant density yields the late-time behaviors  $\delta(t) = 2\gamma(t) \propto t^{-1/4}$ . Consequently,  $F_\nu \propto t^{-\alpha_\nu} \nu^{-\beta_\nu}$  with  $\alpha_\nu = \beta_\nu + 1/2$ , and  $V_{app} = 2\gamma^2 \theta c / (1+z) \propto t^{-1/2}$ , which are all well satisfied by the late-time X-ray afterglow [90] and radio observations of GRB030329 [89]. E.g., the measured spectral index  $\beta_X = 1.17 \pm 0.04$  in the 0.2-10 keV X-ray band [88], yields a late-time temporal decay index  $\alpha_x = \beta_x + 1/2 = 1.67 \pm 0.04$ , in good agreement with the observed  $\alpha_x = 1.67$  [90] as shown in Figure 25. The late time VLBA and VLBI radio measurements of the image-size of GRB030329/SN2003dh are also in good agreement with the CB model prediction.

$$\langle V_{app}(< t) \rangle \approx 2 V_{app}(t) \propto t^{-1/2} \quad (26)$$

This is shown in Figure 26. The CB model prediction is for  $\gamma_0 \theta = 1.76$  obtained from Eq.(22) for the observed [89]  $E_{iso}(GRB030329) \approx (1.86 \pm 0.08) \times 10^{52}$  and  $\langle E_{iso}(OR GRB) \rangle \approx 7 \times 10^{52}$  erg assuming a standard candle GRBs with  $\epsilon_p \approx 1$  eV. The late-time universal behavior,  $V_{app} \propto t^{-1/2}$ , is valid as long as the CB moves within a constant density, independent of the specific values of the density and of  $\epsilon_p$ . The observed late-time behavior shown in Figure 26, suggest deceleration in edge-on host galaxy of a CB with  $\gamma(0) \approx 400$ .

**The FB model** has been used to provide different posteriori interpretations of the observed superluminal expansion [88] of the image size of the source of the radio afterglow of GRB030329/SN2003dh, as the observations progressed. All of them were parametriza-

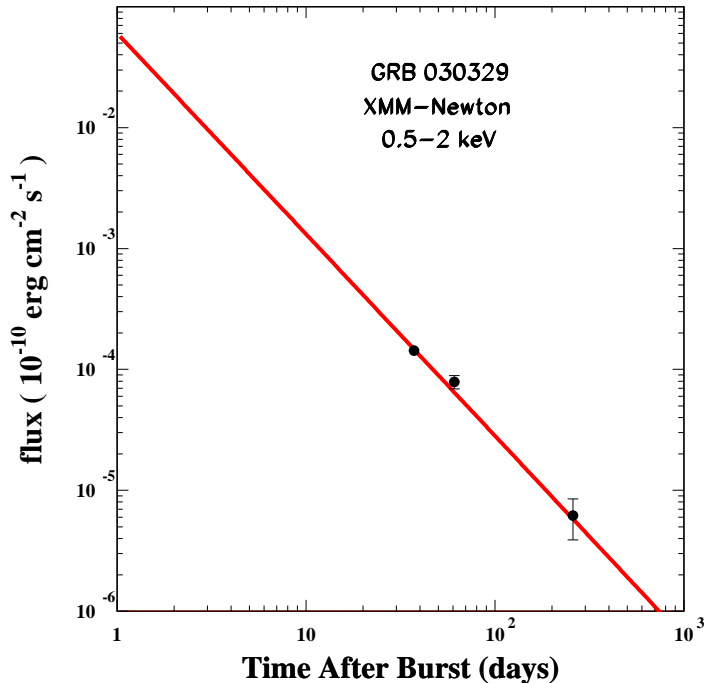


FIG. 25: The late-time 0.5-2 keV X-ray afterglow of the joint source GRB030329/SN2003dh as measured by XMM-Newton [91]. The line is the CB model prediction for the X-ray light-curve assuming that  $\alpha_x = \beta_x + 1/2$  where  $\beta_x = 1.17 \pm 0.04$ .

tions, which depend on many free adjustable parameter rather than falsifiable predictions. Moreover, the radio VLBI observations of SHB170817A show a pointlike (unresolved) radio source displaced at a superluminal speed from the SHB location, rather than an increasing size of a radio image around the location of the SHB as predicted by spherical fireball models or conical fireball models (i.e., structured conical jets) misaligned with respect to the axis of the  $n^*n^*$  binary whose merger produced SHB170817A.

## VI. GRB THEORIES CONFRONT SHB170817A

GW170817 was the first binary neutron-star merger detected with Ligo-Virgo [21] in gravitational waves (GWs). It was followed by SHB170817A,  $1.74 \pm 5$  s [20] after the end of the GWs detection, with an afterglow across the electromagnetic spectrum, which was used to localize it [92] to the galaxy NGC 4993 at a distance of 40 Mpc. The GW170817/SHB170817A association was the first indisputable confirmation that  $n^*n^*$  mergers in compact binaries

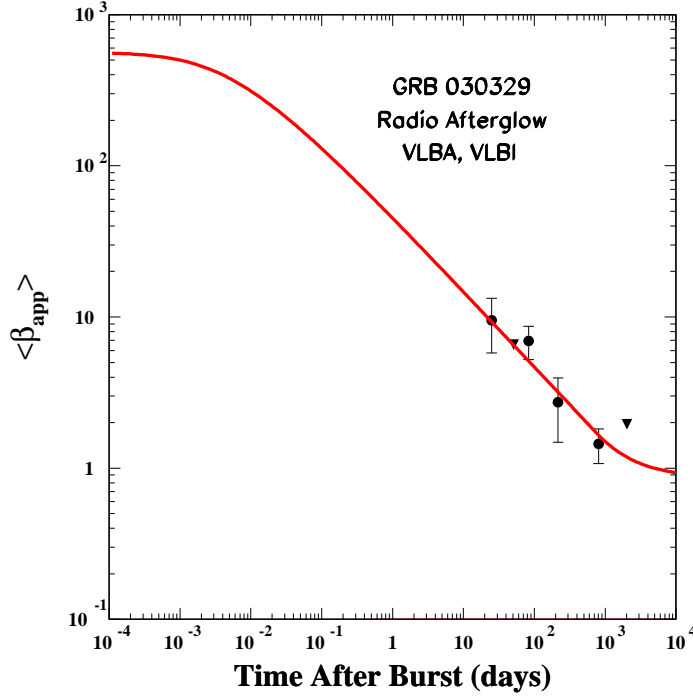


FIG. 26: The time-averaged expansion rate of the radio image of GRB030329/SN2003dh [88]. The line is the predicted  $\langle \beta_{app} \rangle$  of the CB, which produced GRB030329 and its afterglow, assuming that  $2R_{\perp}$  in Eq.(25) is its distance from SN2003dh.

due to GW emission produce GRBs. That was first suggested in 1984 [5] to be due to explosion of the lighter  $n^*$  after tidal mass loss (later called Macornova [6]), and in 1987 due to neutrino annihilation fireball [7] around the remnant  $n^*$ . In 1994, the fireball mechanism was replaced [11] by ICS of external light by a highly relativistic jet of ordinary plasma launched by fall back ejecta on the remnant star after the merger, which became the basis of the CB model of SGRBs and their afterglows.

The relative proximity of SHB170817A provided many critical tests of SGRB theories. Two days before the GW170817/SHB170817A event, the CB model of GRBs was used to predict [93] that most of the SGRBs associated with Ligo-Virgo detections of  $n^*n^*$  mergers will be beamed far off-axis. This is because of beaming and the relatively small volume of the Universe from where  $n^*n^*$  mergers could be detected by the current Ligo-Virgo detectors. Consequently, only a small fraction of them would be visible as low luminosity far off-axis SGRBs [93], while the early time universal afterglow powered by the spin down of the newly

born MSP will produce a characteristic isotropic afterglow with a universal light-curve [22], visible from all SHBs associated with Ligo-Virgo detections of n\*n\* mergers.

Shortly after the detection of the low-luminosity SHB170817A, several authors claimed [81] that SHB170817A was an ordinary near axis SGRB despite its observed smaller  $E_{iso}$  by four orders of magnitude than that of typical SGRBs. Moreover, many authors and promoters of fireball and firecone models, who claimed in the past that ordinary and low luminosity GRBs belong to two different classes of GRB, rushed to suggest the opposite for the low luminosity SHB170817, namely, that it was viewed from far off-axis. This change was not enough, and drastic changes in the FB models were introduced under the cover of "structured jets". Despite the use of many free adjustable parameters, all such models did not predict, rather than predict, correctly the late-time behaviour of the light curve of the afterglow of SHB170817A.

### Test 13: SHB170817A Properties

**Jet Geometry.** The VLBI/VLBA radio observations of the late time radio afterglow [82] of SHB170817A provided the first successful measurement of the the image of the highly relativistic afterglow source of a GRB separated from the GRB and escapes from it with an apparent superluminal speed, as predicted by the CB model already two decades ago [28] in analogy with blazars and microquasar ejections. This is in contrast to the unresolved expanding image of GRB and afterglow [89] advocated by the fireball and firecone models of GRBs and GRB afterglow. This is shown in Figure 27 adapted from [82]. It demonstrates a displacement with time of a point-like source as assumed in the CB model (and seen before in microquasars and blazars [28]), rather than an increasing unresolved joint image of the GRB and its afterglow expected in the FB models and claimed before in the case of GRB030329/SN2003dh [89]. As shown in Figure 27, the angular location of the source of the radio afterglow of SHB170817A has moved in the plane of the sky during  $\Delta t=155$  d (between day 75 and day 230) by  $\Delta\theta_s = 2.68 \pm 0.3$  mas [82].

### Viewing angle from superluminal motion

Assuming a highly relativistic ( $\beta \approx 1$ ) point like radio source, its superluminal velocity satisfies

$$V_{app} \approx \frac{c \sin\theta}{(1+z)(1-\cos\theta)} \approx \frac{D_A \Delta\theta_s}{(1+z)\Delta t}. \quad (27)$$

For an angular distance  $D_A = 39.6$  Mpc to SHB170817A in NGC 4993 at a redshift  $z = 0.009783$  [92], which follows from the local value of the Hubble constant  $H_0 =$

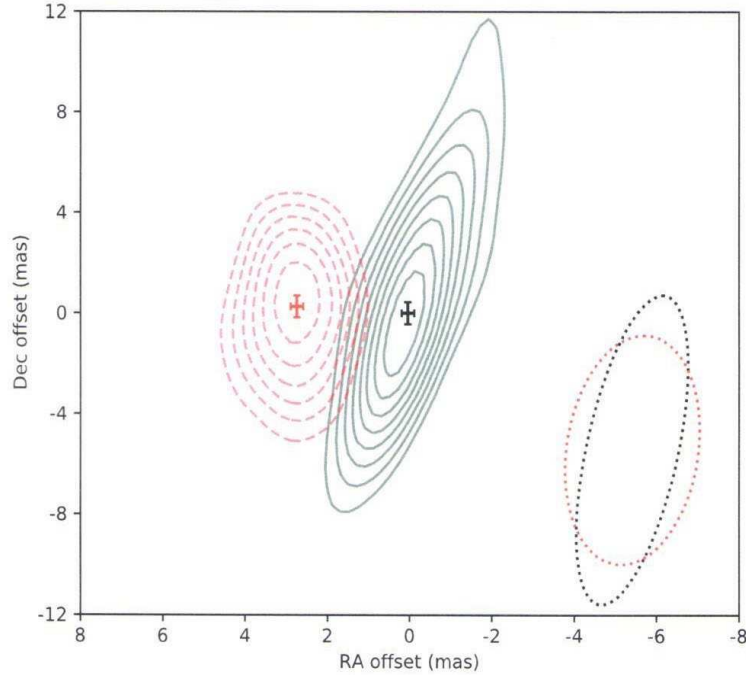


FIG. 27: Proper motion of the radio counterpart of GW170817. The centroid offset positions (shown by  $1\sigma$  errorbars) and  $3\sigma$ - $12\sigma$  contours of the radio source detected 75 d (black) and 230 d (red) post-merger with Very Long Baseline Interferometry (VLBI) at 4.5 GHz. The radio source is consistent with being unresolved at both epochs. The shape of the synthesized beam for the images from both epochs are shown as dotted ellipses to the lower right corner. The proper motion vector of the radio source has a magnitude of  $2.7 \pm 0.3$  mas and a position angle of  $86 \pm 18$  deg over 155 d. The Figure was adapted from [82].

$73.4 \pm 1.62$  km/s/Mpc obtained from Type Ia supernovae [94], and the value  $25 \pm 4$  deg, which was obtained [95] from GW170817 and its electromagnetic location [81,92], Eq.(27) yields  $V_{app} \approx (4.0 \pm 0.40) c$  and consequently  $\theta \approx 28 \pm 2$  deg. This value of the viewing angle  $\theta$  is in agreement with the value  $\theta = 25 \pm 4$  deg, obtained [95] from GW170817 and its electromagnetic location [81,92], assuming the local value of  $H_0$  [94] and that the CB was ejected along the rotation axis of the  $n^*n^*$  binary.

### Initial Lorentz factor

**In the CB model**, SGRBs like LGRBs are assumed to be standard candles viewed from different angles and therefore satisfy similar correlations. In particular, in the CB model,



low luminosity (LL) SHBs such as SHB170817A are ordinary SHBs that are viewed from far off-axis (FOA). Consequently, their  $E_{iso}$  is expected to satisfy,

$$E_{iso}(FOA) \approx \langle E_{iso}(OR) \rangle / [\gamma^2 (1 - \cos\theta)]^3, \quad (28)$$

while

$$(1 + z) E_p(FOA) \approx \langle (1 + z) E_p(OR) \rangle / [\gamma^2 (1 - \cos\theta)]. \quad (29)$$

The measured value  $E_{iso} \approx 5.4 \times 10^{46}$  erg of SHB170817A [96], the mean value  $\langle E_{iso} \rangle \approx 1 \times 10^{51}$  erg of ordinary (OR) SGRBs, and the viewing angle  $\theta \approx 28$  deg obtained from the observed superluminal velocity of the source of its radio afterglow [82], Eq.(29) yields  $\gamma_0 \approx 14.7$  and  $\gamma_0 \theta \approx 7.2$ .

### Radio source size

**In the CB model**, the initial expansion velocity of a CB in its rest frame is  $c/\sqrt{3}$ , the speed of sound in a relativistic gas. In the observer frame

$$V_{exp}(t) \leq \delta c / (1 + z) \sqrt{3} \approx c / (1 + z) \sqrt{3} \gamma (1 - \cos\theta) \quad (30)$$

Consequently, in the CB model, the radius of the CB on day 230 after burst is much below  $2 \times 10^{17}$  cm. At the angular distance of  $D_A = 39.6$  Mpc of NGC 4993, it has an angular size much below the VLBI upper limit  $\approx 1mas$  ( $6 \times 10^{17}$  cm) on the size of the radio source at the distance of NGC 4993 on day 230.

**In the FB models**, the opening angle of the jet has been adjusted to obey the VLBI constraint, but the consistency of the adopted jet structure and the VLBI image has not and could not been demonstrated.

### Prompt Emission Correlations

**In The CB model**, the canonical CB model correlations as given by Eqs.(3),(4) are satisfied well separately by each of the 3 major types of GRBs; SN-LGRBs, SN-less LGRBs and SN-less SGRBs, as was demonstrated in Figures 3,4,5. Eqs.(28),(29) together with the viewing angle of the highly relativistic CB obtained from its apparent superluminal motion [82], allow additional tests of CB model predictions, as follows.

### The peak energy of SHB170817A

Assuming the same redshift distribution of GRBs and SHBs with a mean value  $z \approx 2$ , and the observed mean value  $\langle E_p \rangle = 650$  keV in SHBs [96], yields  $\langle (1+z) E_p \rangle \approx 1950$  keV. Consequently,

Eq.(29) with  $\gamma_0\theta \approx 7.2$  yields  $(1+z)E_p \approx 75$  keV for SHB170817A, compared to  $(1+z)E_p = 82 \pm 23$  keV ( $T_{90}$ ) reported in [20a],  $185 \pm 65$  keV estimated in [20c], and  $E_p \approx 65 + 35 / -14$  keV estimated in [20d], from the same data, with a mean value  $(1+z)E_p = 86 \pm 19$  keV.

In the CB model the peak time  $\Delta t$  after the beginning of a GRB/SHB pulse is roughly equal to half of its FWHM. Assuming that SHBs are roughly standard candles, the dependence of  $\Delta t$  on viewing angle of the CB direction of motion is given by

$$\Delta t(LL \ SHB) \approx \gamma_0^2 (1 - \cos\theta) \langle \Delta t(SHB) \rangle, \quad (31)$$

where  $(SHB)$  stands for OR-SHB. For a viewing angle  $\theta \approx 28$  deg, obtained from the superluminal motion of the resolved source of the late-time radio afterglow of SHB170817A,  $\Delta t \approx 0.58$  s obtained from the prompt emission pulse of SHB170817A (see Figure 9), and  $\langle FWHM(SHB) \rangle = 55$  ms, Eq.(28) yields  $\gamma_0 \approx 14.7$ . This value is consistent with the values obtained from either the estimated  $E_{iso} = 5.4 \times 10^{46}$  of SHB170817A in [81], or the weighted mean value  $E_p = 86 \pm 19$  keV from its estimates in [22].

Moreover, in the CB model the shape of resolved SHB and GRB pulses satisfies  $2 \Delta t \approx FWHM \propto 1/E_p$ . Using the observed  $\langle FWHM(SHB) \rangle \approx 55$  ms and  $\gamma_0 = 14$ , in OR SHBs, and  $\theta \approx 28$  deg, Eq.(31) yields  $\Delta t(SHB170817A) \approx 0.63$  s, in good agreement with its observed value,  $0.58 \pm 0.06$  s.

We caution, however, that replacement of physical parameters by their mean values may be only indicative but not completely reliable, because of detection thresholds, selection effects and wide spread values of physical parameters.

Perhaps the simplest correlation expected in the CB model to be satisfied by resolved pulses of SGRBs is

$$E_p \propto 1/T_p \quad (32)$$

where  $T_p$  is the duration of the pulse (or its peak-time  $\Delta t$ ). This correlation, which is expected to be satisfied also by resolved LGRB pulses, is easier to test in SGRBs because, unlike LGRBs, a large fraction of SGRBs are single pulse SHBs or a sum of very few resolved pulses. Figure 28 compares the predicted correlation  $E_p T_p \approx 100$  keV s and that obtained from the reported values of  $E_p$  and  $T_p$  in the GCN circulars archives, for resolved SGRB pulses measured by the Konus-Wind and by the Fermi-GBM collaborations. As indicated in Figure 28, this CB model correlation seems to be satisfied by most of the measurements, in particular by those with small estimated observational errors.

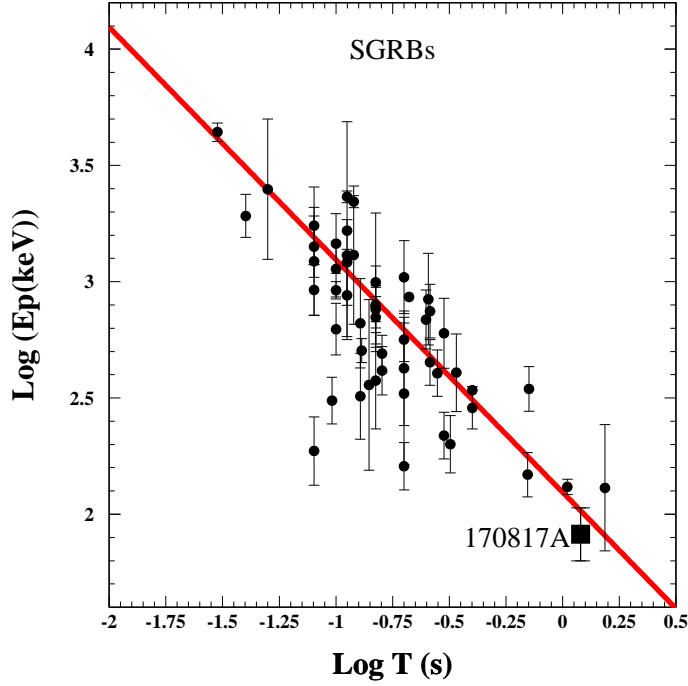


FIG. 28: Comparison between the predicted correlation  $E_p \approx 100 \text{ keV}/(T/s)$  and that obtained from the reported values of  $E_p$  and  $T_p$  in the GCN circular archive for resolved pulses in 54 SGRB pulses measured by the Konus-Wind and Fermi-GBM collaborations.

### The Early Time Afterglow.

The bolometric afterglow of SHB170817A, during the first few days after burst, has the universal shape of the early time X-ray afterglow of all SGRBs and SN-less LGRBs with well sampled X-ray afterglows during the first few days after the prompt emission. This universal shape is that expected from a PWN emission powered by the rotational energy loss of the newly born MSPs in NSMs, through magnetic dipole radiation (MDR), relativistic winds and high energy particles. This was shown For SGRBs in Figure 21. In Figure 29, it is shown separately for the bolometric light curve [71] of SHB170817A during the first two weeks after burst.

### The Late-time Afterglow of SHB170817A.

In the CB model, as long as  $[\gamma(t)]^2 \gg 1$ , and consequently  $\gamma\delta(t) \approx 1/(1-\cos\theta)$ , the spectral energy density of the unabsorbed synchrotron afterglow produced by a CB, which is given

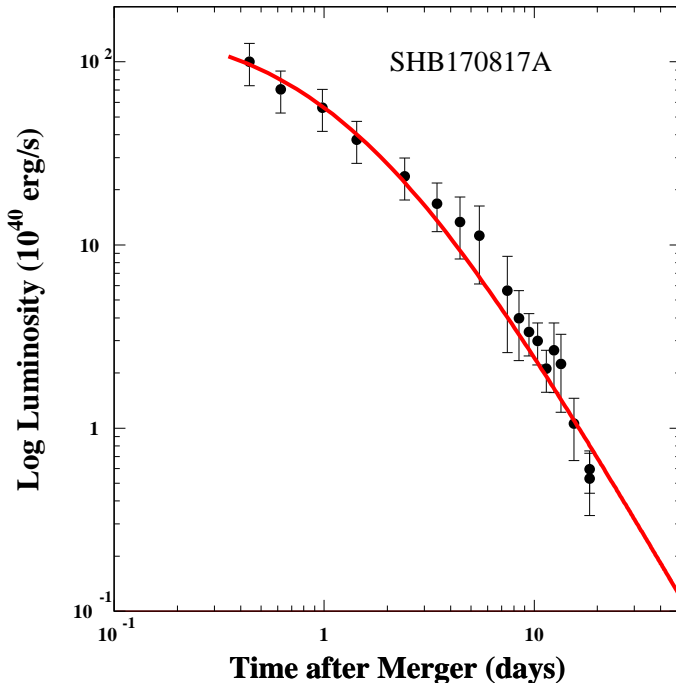


FIG. 29: Comparison between the observed [71] bolometric light curve of SHB170817A and the universal light curve as given by Eq.(21) assuming MSP with  $L(0) = 2.27 \times 10^{42}$  erg/s and,  $t_b = 1.15$  d, with an entirely satisfactory  $\chi^2/dof = 1.04$ .

by Eq.(8), can be rewritten as

$$F_\nu \propto n^{\beta_\nu+1/2} [\gamma(t)]^{1-\beta_\nu/2} \nu^{-\beta_\nu}. \quad (33)$$

In Eq.(33),  $n$  is the baryon density of the external medium encountered by the CB at a time  $t$ , and  $\beta_\nu$  is the spectral index of the emitted synchrotron radiation. For a constant density, the deceleration of the CB yields a late-time  $\gamma(t) \propto t^{-1/4}$  [50], and as long as  $\gamma^2 \gg 1$ ,

$$F_\nu \propto t^{1-\beta_\nu/2} \approx t^{0.73 \pm 0.03}, \quad (34)$$

where we have used the observed value [83]  $\beta_\nu = 0.54 \pm 0.06$ , which extends from the radio (R) through the optical (O) to the X-ray band. When the CB exits the disk of NGC 4993 nearly perpendicular to it, into the halo of the host galaxy, as seems to be the case in SHB170817A [92], the CB deceleration rate diminishes and  $\gamma(t)$  becomes practically constant. Hence, the dependence of  $F_\nu$  on the density turns its increase like  $t^{1-\beta_\nu/2}$  into a fast decay  $\propto [n(r)]^{(1+\beta_\nu)/2}$ . Approximating the disk density as a function of distance  $h$  perpendicular to the disk by

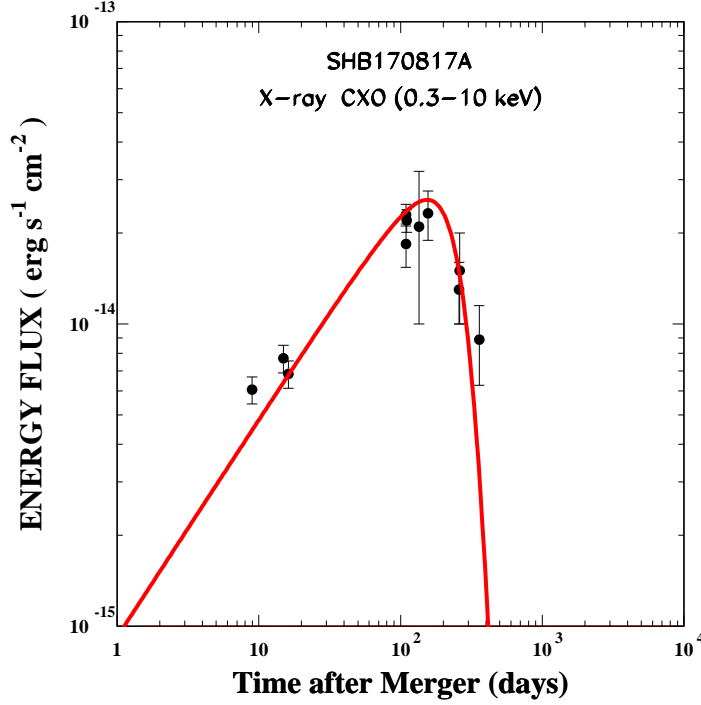


FIG. 30: The light curve of the X-ray afterglow of SHB170817A measured [97] with the CXO and the light curve predicted by eq.(35) for  $\beta_X = 0.56$ ,  $t_e = 245.6$  d and  $w = 63.4$  d.

$n(h) = n(0)/(1 + \exp(h/d))$ , where  $d$  is the "skin depth" of the disk, the light curve of the afterglow of SHB170817A can be approximated by,

$$F_\nu(t) \propto \frac{(t/t_e)^{1-\beta_\nu/2} \nu^{-\beta_\nu}}{[1 + \exp[(t-t_e)/w]]^{(1+\beta_\nu)/2}} \quad (35)$$

where  $t_e$  is roughly the escape time of the CB from the galactic disk into the halo after its launch. The predicted behavior as given by Eq.(35) is compared to the observed late-time X-ray [97] and radio [98] afterglows of SHB170817A in Figures [30] and [31], respectively.

As a further test of the predicted late-time ROX afterglow of SHB170817A by the CB model, we have compared Eq.(35) to the late-time observations of its optical afterglow with the Hubble Space Telescope, which extended until one year after burst [99]. This is shown in Figure 32.

### FB Model Interpretations

Soon after the discovery of the rising late-time radio, optical and X-ray afterglows of SHB170817A, many versions of FB models and postdicted rising light curves began to flood

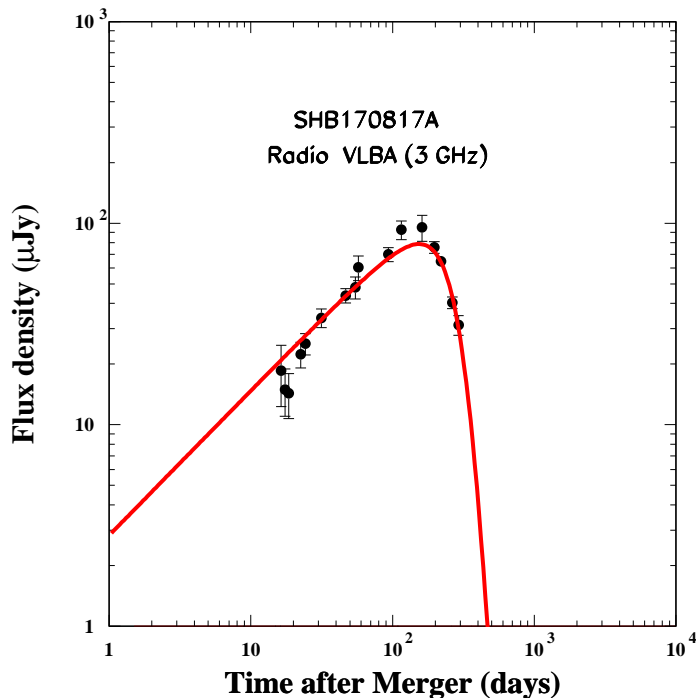


FIG. 31: The measured [98] light curve of the radio afterglow of SHB170817A at 3 GHz compared to the light curve predicted by eq.(35) with  $\beta_r = 0.56$ ,  $t_e = 245.6$  d and  $w = 63.4$  d.

the arXiv and the leading astrophysical journals. In fact, all the predicted FB model light curves turned out later to be failures, despite the fact that they involved many parameters and free choices, which were adjusted by best fit to the available data at the time of publication. Below, we shall demonstrate a couple of such repeated failed efforts by astrophysicists and observers, promoters of the FB model.

Consider first Figure 33 (Figure 1 adapted from [100]). It summarizes a consensus posted in November 2017 by 25 authors who include main leading observers and astrophysicists, promoters of the FB models of GRBs, who have concluded that "the off axis jet scenario as a viable explanation of the radio afterglow of SHB170817A is ruled out" and a choked jet cocoon model is most likely the origin of gamma rays and afterglow of SHB170817A. Figure 34 (Figure 3 adapted from [100]) presents the "observational support" there for their claim that "the off axis jet scenario as a viable explanation of the radio afterglow of SHB170817A is ruled out" on the basis of their shown best fits to the 3 GHz radio data obtained before November 2017. Figure 35 (Figure 1 adapted from [101]) presents a best fit smoothed

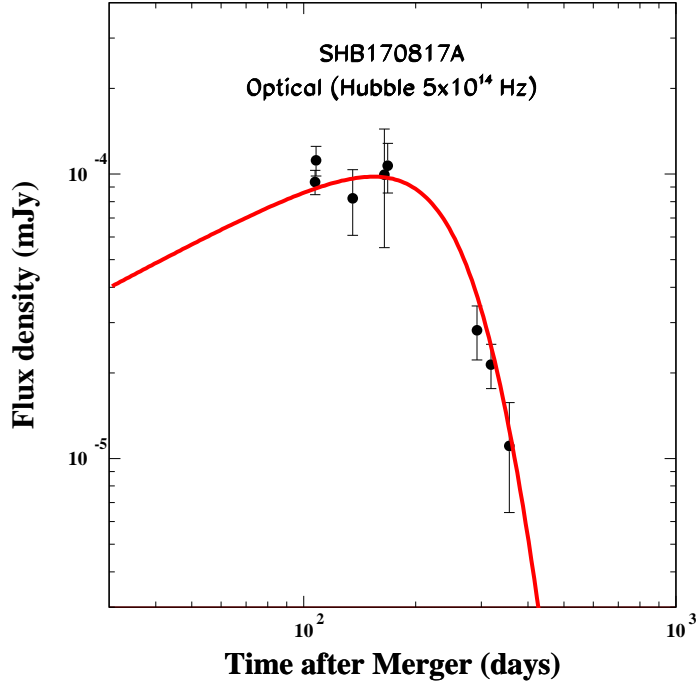


FIG. 32: The measured late-time light curve of the optical afterglow of SHB170817A with the Hubble space telescope [99] at  $3.8 \times 10^{14}$  Hz and  $5.1 \times 10^{14}$  Hz compared to the light curve predicted by eq.(35) with  $\beta = 0.56$ ,  $t_e = 245.6$  d and  $w = 63.4$  d. ( $\chi^2/dof = 0.88$ ).

broken power-law to the light curve of SHB170817A. The data is from ATCA (circles) and VLA (squares) observations. Unlike [100]. Figure 36 (Figure 2 adapted from [102]) summarizes the 0.6-10 GHz observations of the radio afterglow of SHB170817A covering the period up to 300 days post-burst, taken with the upgraded Karl G. Jansky Very Large Array, the Australia Telescope Compact Array, the Giant Metrewave Radio Telescope and the MeerKAT telescope. On the basis of these data and its parametrization as a smoothed broken power-law [103] with a temporal index  $\alpha = 0.84 \pm 0.05$  on the rise, peak time  $149 \pm 2$  day, and a temporal index  $1.6 \pm 0.2$  on the decay, the authors of [102] now concluded that these data consist "Strong Jet Signature in the Late-Time Lightcurve of GW170817" in contrast to . The authors justify their conclusion by the fact that a flux density  $F_\nu(t) \propto t^\alpha \nu^\beta$  with the observed  $\beta = 0.54$  and the observed values of  $\alpha$ , both before and after the temporal break, cannot be produced by a spherical relativistic fireball [102]. On the other hand, for a jet viewed on-axis after the jet-break, the power-law decay index is  $\alpha = -p$  where  $\beta = (1-p)/2$

Mooley (1,2,3,19), Nakar (4), Hotokezaka (5),  
Hallinan (3), Corsi (6), Frail (2), Horesh (7),  
Murphy (8,9), Lenc (8,9), Kaplan (10),  
De (3), Dobie (8,9,11), Chandra (12,13),  
Deller (14), Gottlieb (4), Kasliwal (3),  
Kulkarni (3), Myers (2), Nissanke (15),  
Piran (7), Lynch (8,9), Bhalerao (16),  
Bourke (17), K.W. Bannister (11),  
L.P. Singer (18)

- 
- (1) Hintze Fellow, Oxford,
  - (2) NRAO,
  - (3) Caltech,
  - (4) Tel Aviv University,
  - (5) Princeton University,
  - (6) Texas Tech University,
  - (7) The Hebrew University of Jerusalem,
  - (8) University of Sydney,
  - (9) CAASTRO,
  - (10) University of Wisconsin - Milwaukee,
  - (11) ATNF, CSIRO,
  - (12) NCRA,
  - (13) Stockholm University,
  - (14) Swinburne University of Technology,
  - (15) Radboud University,
  - (16) IIT Bombay,
  - (17) Chalmers University of Technology,
  - (18) NASA GSFC,
  - (19) Jansky Fellow, NRAO/Caltech

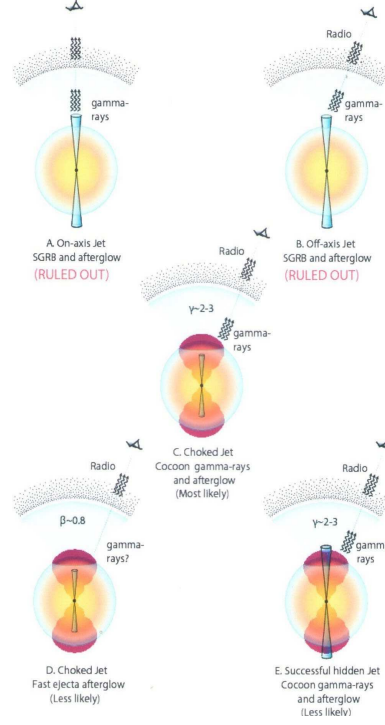


FIG. 33: Figure 2 adapted from [100] is a cartoon representing the consensus of 25 authors, who include many leading observers and many other promoters of the FB models of GRBs who posted it in November 2017. They concluded that "the off axis jet scenario as a viable explanation of the radio afterglow of SHB170817A is ruled out" while "a choked jet cocoon model is most likely the origin of gamma rays and afterglow of SHB170817A".

[104], i.e.,  $p=2.17$  for SHB170817A, consistent with that observed. However,

(a) The last result is valid only for an hypothesized fast spreading jet, i.e. a conical jet with a fast lateral expansion ( $V_{\perp} \approx c$  in the jet rest frame at the jet break time [104], which stops its propagation). This is not supported by the VLBI observations of the radio afterglow of SHB170817A [82], which show a compact superluminal source (CB) rather than a spreading conical flow with an expanding large opening angle.

(b) The relation  $\alpha = -p = 1 - 2\Gamma$ , where  $\Gamma$  is the post break photon index, is seldom satisfied in LGRBs and often yields unacceptable  $p < 2$ . Due to a large uncertainty, it is not clear yet whether the late-time afterglow of SHB170817A can be really parametrized well by a broken power-law.

All types of fireball, firecone, or structured jet models, which have been claimed in



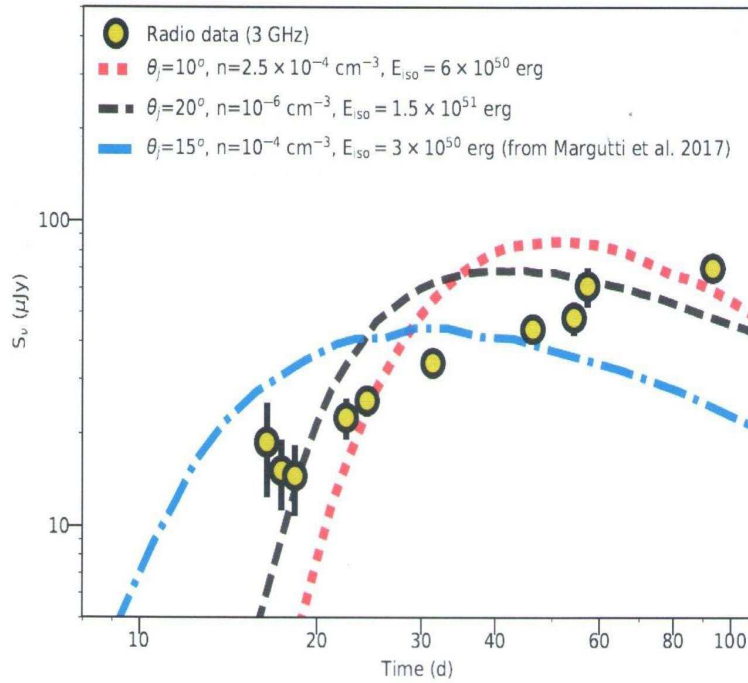


FIG. 34: Best fit light curves to the observed 3 GHz radio afterglow of SHB170817A measured until the end of October 2017 [100], based on far off-axis jet models. These fits were used in [100] to conclude that "the off axis jet scenario as a viable explanation of the radio afterglow of SHB170817A is ruled out".

either posted papers in the arXive, or submitted papers for publication in journals, failed to predict correctly the observed light curves after the posting or or submission for publication of these papers. This is demonstrated in Figures 37. In Figure 37 Top (Figure 1. adapted from V2 of [105]) a structured jet with a relativistic, energetic core surrounded by slower and less energetic wings produces an afterglow emission that brightens characteristically with time, as was seen in the afterglow of SHB170817A in 2017, and was postdicted. It was argued that, initially, one sees only the relatively slow material moving towards us. As time passes, larger and larger sections of the outflow become visible, increasing the luminosity of the afterglow. In the last revised version (V4) of [105], the postdicted light curves in Figure 37 top were replaced by best fits to the measured radio, optical and X-ray light curve until 250 days after burst (March 2018) shown in Figure 37 bottom (Figure 2 adapted from [106], the final published version of [105]).

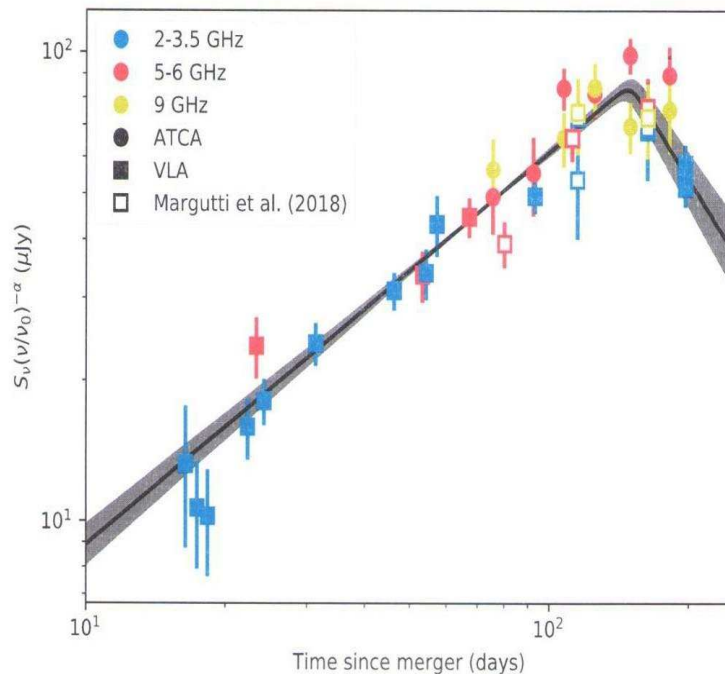


FIG. 35: Figure 1 adapted from [101] show the radio light curve of SHB170817A from ATCA (circles) and VLA (squares) observed before March 3, 2018, and grouped by frequency band [101]. The flux densities have been adjusted to 5.5 GHz assuming a spectral index  $-0.57 \pm 0.04$ . Shown also is a best fit smoothed broken power-law with a temporal index  $0.84 \pm 0.05$  on the rise, peak time  $149 \pm 2$  d, and a temporal index  $1.6 \pm 0.2$  on the decay.

Despite reproducing light curves with many free adjustable parameters, conical jets with standard lateral structures have not been shown capable of reproducing cannonball-like VLBI radio images displaced with a superluminal velocity from the location of SHB170817A, as was observed [82] between day 75 and 230 after burst [82].

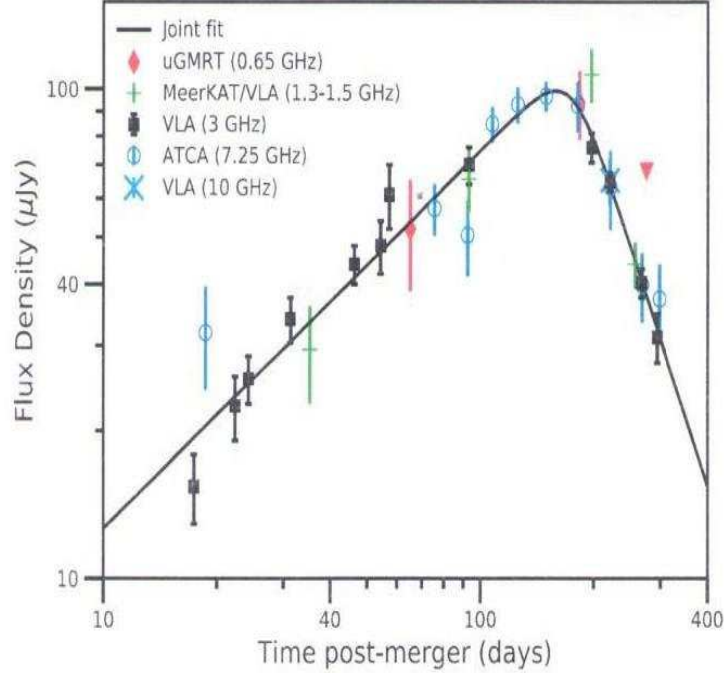


FIG. 36: Figure 2 adapted from [102]. The radio light curve of SHB170817A, measured until June 12, 2018, spanning multiple frequencies, and scaled to 3 GHz using the spectral index  $-0.53$ . Shown also is a best fit smoothly broken power-law parametrization [103] with five adjustable parameters.

## VII. CONCLUSIONS

Table III summarizes the confrontations of the key falsifiable predictions of the fireball and cannonball models of GRBs, with observations rather than with prejudices and beliefs. They clearly demonstrate that more than 50 years after the discovery of GRBs, the minority views on GRBs continue to be the correct views. This is summarized briefly in Table IV. It has been obscured, however, by the continuous flow of uncritical papers and reviews of GRBs by biased followers and promoters of the fireball model [27]. Moreover, whenever it became clear from observations that a minority view is the correct view, it was adapted/incorporated into the FB model without much ceremony, proper references, and due credit to its true origin!

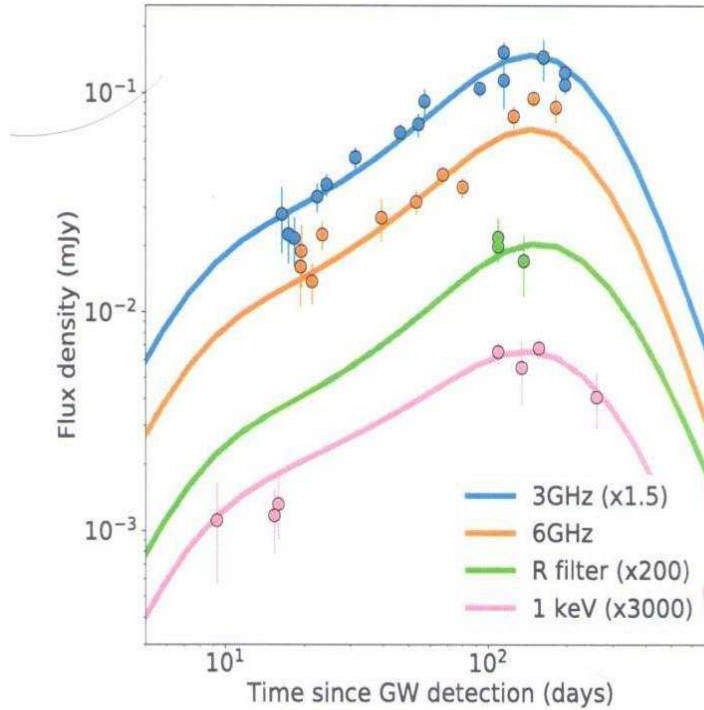
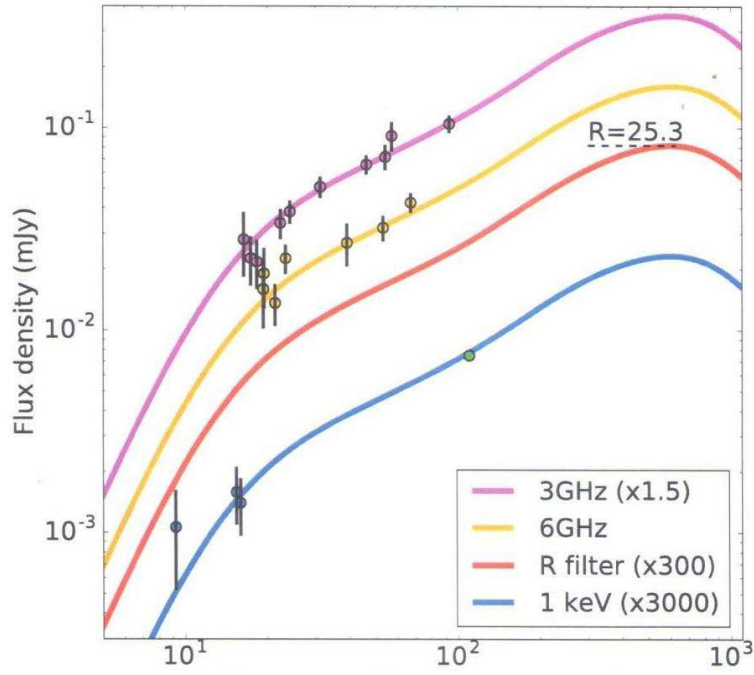


FIG. 37: Top: Best fit radio, optical and X-ray (ROX) light curves of an off-axis structured jet model reported in [105] to the ROX afterglows of SHB170817A measured before December 2017. Bottom: Best fit light curves to the observed ROX afterglow of SHB170817A until April 2018, obtained from a structured jet model and reported in [106] (Figure 2 in version 4 of [105]).

- 
- [1] G.J. Fishman, C.A. Meegan, *ARA&A*, 33 (1995) 415.
- [2] R.W. Klebesadel, I.B. Strong, R.A. Olson, *ApJ*, 182 (1973) L85.
- [3] R.J. Nemiroff, *ComAp*, 17 (1994) 189 [arXiv:astro-ph/9402012].
- [4] J.P. Norris, et al., *Nature*, 308, (1984) 434  
C. Kouveliotou, et al., *ApJ*, 413 (1993) L101 (1993).
- [5] S.I. Blinnikov, et al. *SAL*, 10 (1984) 177 [arXiv:1808.05287].
- [6] B. Paczynski, *ApJ*, 308 (1986) L43.
- [7] J. Goodman, A. Dar, S. Nussinov, *ApJ*, 314 (1987) L7.
- [8] J. Goodman, *ApJ*, 308 (1986) L47.
- [9] C.A. Meegan, et al., *Nature*, 355 (1992) 143.
- [10] M.J. Rees, P. Meszaros, *MNRAS*, 25 (1992) 29
- [11] N. Shaviv, A. Dar, *ApJ*, 447 (1995) 863 [arXiv:astro-ph/9407039].
- [12] B. Paczynski, J.E. Rhoads, *ApJ*, 418 (1993) 5 [arXiv:astro-ph/9307024].  
J.I. Katz, *ApJ*, 432 (1994) L107 [arXiv:astro-ph/9312034].  
P. Meszaros, M.J. Rees, *ApJ* 476 (1997) 232 [arXiv:astro-ph/9606043].
- [13] E. Costa, et al., *Nature*, 38 (1997) 783 [arXiv:astro-ph/9706065].
- [14] J. van Paradijs, et al., *Nature*, 386 (1997) 686.  
D.A. Frail, et al., *Nature*, 389 (1997) 261.
- [15] K.C. Sahu, et al., *Nature*, 387 (1997) 476 [arXiv:astro-ph/9705184].
- [16] M.R. Metzger, S.G. Djorgovski, S.R. Kulkarni, et al., *Nature*, 387 (1997) 878.
- [17] T.J. Galama, et al., *Nature*, 395 (1998) 670 [arXiv:astro-ph/9806175].
- [18] See, e.g., J.P.U. Fynbo, D. Malesani, P. Jakobsson, in "Gamma-Ray Bursts", Cambridge Astrophysics Series 51, pp. 269-290 (2012) and references therein.
- [19] W. Fong, E. Berger, *ApJ*, 776 (2013) 18 [arXiv:1307.0819]  
E. Berger, *ARA&A*, 52 (2014) 43 [arXiv:1311.2603].
- [20] A. von Kienlin, et al., 2017, GCN Circular 21520.  
A. Goldstein, A., et al. 2017, GCN Circular 21528.  
A. Goldstein, et al., *ApJ*, 848 (2017) L14 [arXiv:1710.05446].  
A.S. Pozanenko, et al., *ApJ*, 852 (2018) 30 [arXiv:1710.05448].

- V. Savchenko, et al., *ApJ*, 848 (2018) L15 [arXiv:1710.05449].
- [21] B.P. Abbott, et al. (Ligo-Virgo Collaboration), *Nature* 551 (2017) 85 [arXiv:1710.05835].  
 B.P. Abbott, et al. (Ligo-Virgo Collaboration) *ApJ*, 848 (2017), L13 [arXiv:1710.05834].  
 B.P. Abbott, et al. (Ligo-Virgo Collaboration) *PRL*, 119 (2017) 161101 [arXiv:1710.05832]  
 B.P. Abbott, et al. (Ligo-Virgo Collaboration) *ApJ*, 848 (2017) [arXiv:1710.05833].
- [22] S. Dado, A. Dar, 2018 [arXiv:1807.08726].
- [23] A. Melandri, et al., *A&A*, 567 (2014) A29 [arXiv:1404.6654].  
 Z. Cano, et al., *AdAst* (2017), 5c (arXiv:1604.03549), and references therein.
- [24] A. Gal-Yam, et al., *Nature*, 444 (2006) 1053 [arXiv:astro-ph/0608257].  
 J.P.U. Fynbo, et al., *Nature*, 444 (2006)1047 [arXiv:astro-ph/0608313].
- [25] S. Dado, A. Dar, 2018 [arXiv:1808.08912].
- [26] S. Dado, A. Dar, *ApJ*, 855 (2018) 88 [arXiv:1710.02456].
- [27] A partial list of reviews include:  
 T. Piran, *Phys. Rep.* 314 (1999) 575 [arXiv:astro-ph/9810256].  
 T. Piran, *Phys. Rep.*, 333 (2000) 529 [arXiv:astro-ph/9907392].  
 P. Meszaros, *ARA&A*, 40 (2002) 137 [arXiv:astro-ph/0111170].  
 T. Piran *Rev. Mod. Phys.* 76 (2004) 1143 [arXiv:astro-ph/0405503].  
 B. Zhang, P. Meszaros, *Int. J. Mod. Phys. A*, 19 (2004) 2385 [astro-ph/0311321].  
 P. Meszaros, *Rep. Prog. Phys.* 69 (2006) 2259 [arXiv:astro-ph/0605208].  
 B. Zhang, *Chin. J. Astron. Astrophys.* 7 [2007] 1 [arXiv:astro-ph/0701520].  
 E. Nakar, *Phys. Rep.* 442 (2007) 166 [astro-ph/0701748].  
 E. Berger, *ARA&A*, 52 (2014) 43 [arXiv:1311.2603].  
 P. Meszaros, M.J. Rees, 2014 [arXiv:1401.3012].  
 A. Pe'er, *AdAst*,(2015) Vol. 2015, 22 [arXiv:1504.02626].  
 P. Kumar, B. Zhang, *Phys. Rep.* 561 (2015) 1 [arXiv:1410.0679].  
 Z. Dai, E. Daigne, P. Meszaros, *SSRv*, 212 (2017) 409.
- [28] N.J. Shaviv, A. Dar, *ApJ* 447 (1995) 863 [arXiv:astro-ph/9407039].  
 Dar, *ApJ*, 500 (1998) L93 [arXiv:astro-ph/9709231].  
 A. Dar *A&AS*, 138 (1999) 505 [arXiv:astro-ph/9902017].  
 A. Dar, R. Plaga, *A&A* 349 (1999) 259 [arXiv:astro-ph/9902138].  
 A. Dar, A. De Rújula, 2000 [arXiv:astro-ph/0012227].

- S. Dado, A. Dar, A. De Rújula, *A&A*, 388 (2002) 1079D [arXiv:astro-ph/0107367].
- A. Dar, A. De Rújula, *Phys. Rep.* 405 (2004) 203 [arXiv:astro-ph/0308248].
- S. Dado, A. Dar, A. De Rújula, *ApJ*, 696 (2009) 994 [arXiv:0809.4776] and references therein.
- [29] K.M. Popper, *The Logic of Scientific Discovery*, Rout-ledge Classics 1959.
- [30] S. Dado, A. Dar, 2018 [arXiv:1808.08912].
- [31] P. Meszaros, M.J. Rees, 2014 [arXiv:1401.3012].
- [32] S.E. Woosley, *A&AS*, 97 (1993) 205.
- [33] S.E. Woosley, *ApJ*, 405 (1993) 273.
- [34] A.I. MacFadyen, S.E. Woosley, *ApJ*, 524 (1999) 262 [arXiv:astro-ph/9810274].
- [35] S.I. Blinnikov, et al., *PAZh*, 10 (1984) 422
- S.I. Blinnikov, et al. *SvAL*, 10 (1984) 177 [arXiv:1808.05287].
- L.X. Li, B. Paczynski, *AJ*, 507 (1998) L59 [arXiv:astro-ph/9807272].
- [36] N.J. Shaviv, A. Dar, *ApJ* 447 (1995) 863 [arXiv:astro-ph/9407039].
- A. Dar, A. De Rújula, *Phys. Rept.* 405 (2004) 203 [arXiv:astro-ph/0308248].
- [37] See, e.g., S. Covino, D. Gotz, *A&AT*, 29 (2016) 205 [arXiv:1605.03588].
- [38] W. Coburn, S.E. Boggs, *Nature* 423 (2003) 415 [arXiv:astro-ph/0305377].
- D.R. Willis, E.J. Barlow, A.J. Bird, *A&A*, 439 (2005) 245 [arXiv:astro-ph/0505097].
- E. Kalemci, et al. *ApJS*, 169 (207) 75 [arXiv:astro-ph/0610771].
- D. Yonetoku, et al., *ApJ* 743 (2011) L30 [arXiv:1111.1779].
- D. Yonetoku, et al., *ApJ*, 758(2012) L1 [arXiv:1208.5287].
- D. Gotz, et al., *MNRAS*, 431 (2013) 3550 [arXiv:1303.4186].
- D. Gotz, P. Laurent, S. Antier, et al., *MNRAS*, 444 (2014) 2776 [arXiv:1408.4121].
- [39] E.E. Fenimore, C.D. Madras, S. Nayakshin, *AJ*, 473 (1996), 998 [arXiv:astro-ph/9607163].
- P. Kumar, A. Panaitescu, 2000, *ApJ*, 541 (2000), L51 [arXiv:astro-ph/0006317].
- F. Ryde, V. Petrosian, *A.J.* 578 (2002), 290 [arXiv:astro-ph/0206204].
- D. Kocevski, F. Ryde, E. Liang, *ApJ*, 596 (2003) 389 [arXiv:astro-ph/0303556].
- C.D. Dermer, *ApJ*, 614 (2004) 284, [arXiv:astro-ph/0403508].
- E.W. Liang, et al., *ApJ*, 646 (2006) 351 [arXiv:astro-ph/0602142].
- A. Panaitescu, *NC*, B121 (2006) 1099 [arXiv:astro-ph/0607396].
- [40] A. Dar, A. De Rújula, 2000 [arXiv:astro-ph/0012227].

- [41] L. Amati, F. Frontera, M. Tavani, et al., *A&A*, 390 (2002) 81 [arXiv:astro-ph/0205230].
- [42] See, e.g., S. Dado, A. Dar, A. De Rújula, *ApJ*, 696 (2009) 994 [arXiv:0809.4776] for LGRBs.  
S. Dado, A. Dar, [arXiv:1808.08912], for SHBs.
- [43] D. Kocevski, F. Ryde, E. Liang, *ApJ*, 596 (2003) 389 [arXiv:astro-ph/0303556].
- [44] S. Kobayashi, T. Piran, R. Sari, *ApJ*, 490 (1997) 92 [arXiv:astro-ph/9705013].
- [45] J.P. Norris, et al., *ApJ*, 627 (2005) 324 [arXiv:astro-ph/0503383].  
J. Hakkila<sup>1</sup>, et al., *ApJ*, 815 (2015)134 [arXiv:1511.03695].
- [46] S. Dado, A. Dar, A. De Rújula, *A&A*, 388 (2002) 1079 [arXiv:astro-ph/0107367].  
S. Dado, A. Dar, A. De Rújula, *ApJ*, 646 (2006) L21, [arXiv:astro-ph/0512196].
- [47] J.A. Nousek, et al., *ApJ*. 642 (2006) 389 [arXiv:astro-ph/0508332].
- [48] S. Vaughan, et al., *ApJ*, 638 (2006) 920 [arXiv:astro-ph/0510677].
- [49] G. Cusumano, et al., *ApJ*, 639 (2006) 316 [arXiv, astro-ph/0509689].
- [50] S. Dado, A. Dar, *A&A*, 558 (2013) A115 [arXiv:1303.2872].
- [51] Swift-XRT GRB light curve repository, UK Swift Science Data Centre, Univ. of Leicester  
P.A. Evans, et al., *A&A*, 469 (2007) 379 [arXiv:0704.0128].  
P.A. Evans, et al., *MNRAS*, 397 (2009) 1177 [arXiv:0812.3662].
- [52] M. De Pasquale, M.J. Page, D.A. Kann, et al., *MNRAS* 462 (2016) 1111 [arXiv:1602.04158].
- [53] A. Maselli, et al., *Science*, 343, (2014) 48 [arXiv:1311.5254].
- [54] D. Grupe, et al., *ApJ*, 711 (2010) 1008 [arXiv:0903.1258].
- [55] S. Dado, A. Dar, A. De Rújula, *ApJ*, 680 (2008) 517 [arXiv:0712.1527].
- [56] P. Schady, M. de Pasquale, M.J. Page, et al., 2007, *MNRAS*, 380 (2007) 1041  
[arXiv:astro-ph/0611089].
- [57] S. Dado, A. Dar, *PhRvD*, 94 (2016) 3007 [arXiv:1603.06537].
- [58] R.A.M. Wijers, M. J. Rees, P. Meszaros, *MNRAS*, 288 (1997) L51 [arXiv:astro-ph/9704153].
- [59] P. Meszaros, M.J. Rees, *ApJ* 476 (1997) 232 [arXiv:astro-ph/9606043].
- [60] e.g, T. Piran, *Phys. Rep.* 314 (1999) 575 [arXiv:astro-ph/9810256].
- [61] R. Sari, T. Piran, R. Narayan, *ApJ*, 497 (1998) L17 [arXiv:astro-ph/9712005].
- [62] E.G. Blackman, I. Yi, *ApJ*, 498 (1998) L31 [arXiv:astro-ph/9802017].  
Z.G. Dai, T. Lu, *PRL*, 81 (1998) 4301 [arXiv:astro-ph/9810332].  
Z.G. Dai, T. Lu, *A&A*, 333 (1998) L87 [arXiv:astro-ph/9810402].  
B. Zhang, P. Meszaros, *ApJ*, 552 (2001) L35 [arXiv:astro-ph/0011133].



- Z.G. Dai et al., *Science* 311, 1127 (2006), [arXiv:astro-ph/0602525].
- B.D. Metzger, E. Quataert, T.A. Thompson, *MNRAS*, 385 (2008) 1455 [arXiv:0712.1233].
- B.P. Gompertz, P.T. O'Brien, G.A. Wynn, *MNRAS*, 438 (2014) 240 [arXiv:1311.1505].
- B.D. Metzger, A. L. Piro, *MNRAS*, 439 (2014) 3916 [arXiv:1311.1519].
- H. Lu, et al., *MNRAS*, *ApJ*, 805 (2015) 89 [arXiv:1501.02589].
- S. Gibson, et al., *MNRAS*, 470 (2017) 4925 [arXiv:1706.04802].
- [63] J.E. Rhoads, *ApJ*, 525 (1999) 737 [arXiv:astro-ph/9903399].
- R. Sari, T. Piran, J.P. Halpern, *ApJ*, 519 (1999) L17 [arXiv:astro-ph/9903339].
- [64] D.A. Frail, et al., *ApJ*, 562 (2001) L55 [arXiv:astro-ph/0102282].
- [65] R.A. Chevalier, Z.Y. Li, *ApJ*, 536 (2000) 195 [arXiv:astro-ph/9908272].
- J.S. Bloom, D.A. Frail, S.R. Kulkarni, *ApJ*, 594 (2003) 674 [arXiv:astro-ph/0302210].
- [66] S. Dado, A. Dar, *A&A*, 558 (2013) 115 [arXiv:1303.2872].
- [67] E.W. Liang, et al., *ApJ*, 675 (2008) L528 [arXiv:0708.2942].
- [68] J.L. Racusin, et al., *ApJ*, 698 (2009) 43 [arXiv:0812.4780].
- [69] E. Pian, et al., *A&A*, 372 (2001) 456 [arXiv:astro-ph/0012107].
- [70] K.Z. Stanek, et al., *ApJ*, 522 (1999) L39 [arXiv:astro-ph/9905304].
- F. Harrison, et al., *ApJ*, 523 (1999) L121 [arXiv:astro-ph/9905306].
- G.L. Israel, et al., *A&A*, 348, (1999) L5 [arXiv:astro-ph/9906409].
- K. Beuermann, et al., 1999, *A&A*, 352, L26 [arXiv:astro-ph/9909043].
- [71] M.R. Drout, et al., *Science*, 358 (2017) 1570 [arXiv:1710.054431].
- [72] R.A.M.J. Wijers, et al., *MNRAS* (1998) 294, L13 [arXiv:astro-ph/9708183].
- D.W. Hogg, A.S. Fruchter, *ApJ*, 520 (1999), 54 [arXiv:astro-ph/9807262].
- [73] S. Dado, A. Dar, *ApJ*, 785 (2014) 70 [arXiv:1307.5556].
- [74] D. Guetta, M. Della Valle, *ApJ*, 657 (2007) L73 [arXiv:astro-ph/0612194].
- [75] F. Daigne, E.M. Rossi, R. Mochkovitch, *MNRAS*, 372 (2006) 1034D [arXiv:astro-ph/0607618].
- T. Le, C.D. Dermer, *ApJ*, 661 (2007) 394 [arXiv:astro-ph/0610043].
- H. Yuksel, M.D. Kistler, *PhRvD*, 75 (2007) 3004 [arXiv:astro-ph/0610481].
- R. Salvaterra, G. Chincarini, *ApJ* 656 (2007) L49 [arXiv:astro-ph/0612278].
- L.X. Li, *MNRAS*, 388 (2008) 1487 [arXiv:0710.3587].
- M.D. Kistler et al., *ApJ*, 673 (2008) L119 [arXiv:0709.0381].

- H. Yuksel, et al., *ApJ*, 683 (2008) L5 [arXiv:0804.4008].
- R. Salvaterra, et al., *MNRAS*, 396 (2009) 299 [arXiv:0805.4104].
- [76] A.M. Soderberg, et. al., *Nature*, 430 (2004) 648 [arXiv:astro-ph/0408096].
- D.M. Coward, *MNRAS*, 360, (2005) L77 [arXiv:astro-ph/0504493].
- E. Pian, et al., *Nature*, 442 (2006) 1011 [arXiv:astro-ph/0603530].
- B.E. Cobb, et al., *ApJ*, 645 (2006) L113 [arXiv:astro-ph/0603832].
- E. Liang, et al., *ApJ*, 662 (2007) 1111 [arXiv:astro-ph/0605200].
- L. Amati, et al., *A&A* 463 (2007) 913 [arXiv:astro-ph/0607148].
- A.M. Soderberg, et al., *ApJ*, 661 (2007) 982 [arXiv:astro-ph/0607511].
- D. Guetta, M. Della Valle, *ApJ* 657 (2007) L73 (arXiv:astro-ph/0612194]
- F. Virgili, E.W. Liang, B. Zhang, *MNRAS*, 392 (2009) 91 [arXiv:0801.4751].
- Y. Z. Fan, et al., *ApJ* 726 (2011) 32 [(arXiv:1004.5267].
- O. Bromberg, et al., *ApJ*, 739 (2011) L55 [arXiv:1107.1346].
- [77] D. Guetta, T. Piran, *JCAP*, 07 (2007) 003 [arXiv:astro-ph/0701194].
- B.E. Robertson, & R.S. Ellis *ApJ*, 744, (2012) 95 [arXiv:1109.0990].
- J.J. Wei, et al *MNRAS*.439 (2014) 33 [arXiv:1306.4415].
- [78] L. Amati, *MNRAS*, 372 (2006) 233 [arXiv:astro-ph/0601553].
- [79] E. Pian, et al., *AdSpR*, 34 (2004) 2711 [arXiv:astro-ph/0304521].
- [80] R.A. Kulkarni, et al., *Nature*, 395, 663 (1998).
- C. Kouveliotou, et al., *ApJ*, 608 (2004) 972 [arXiv:astro-ph/0401184].
- [81] [81] A. Goldstein, et al., *ApJ*, 848 (2017) L14 [arXiv:1710.05446].
- [82] K.P. Mooley, et al., *Nature* 561 (2018) 355 [arXiv:1806.09693].
- [83] K.P. Mooley, et al., *ApJ*, 868 (2018) L11 [arXiv:1810.12927].
- [84] J.C. Kapteyn, 1902, *Astron. Nachr.*, 157 (1902) 201.
- [85] M.J. Rees, *Nature*, 211 (1966) 468.
- [86] A. Dar, A. De Rújula, 2000 [arXiv:astro-ph/0008474].
- S. Dado, A. Dar, A. De Rújula, 2016 [arXiv:1610.01985].
- [87] A.M. Soderberg, et al., *ApJ* 607 (2004) L13 [arXiv:astro-ph/0402163].
- [88] P.N. Bhat, et al., 744 (2012) 141 [arXiv:1109.4064].
- [89] G.B. Taylor, et al., *ApJ*, 609 (2004) L1.
- G.B. Taylor, et al., *ApJ*, 622 (2005) 986.

- Y.M. Pihlstrom, et al., *ApJ*, 664 (2007) 411 [arXiv:0704.2085].
- R.A. Mesler, et al., , *ApJ*, 759 (2012) 4 [arXiv:1208.3643].
- R.A. Mesler, Y.M. Pihlstrom, *ApJ*, 774 (2013) 77 [arXiv:1304.3858].
- [90] R. Vanderspek, et al., *ApJ*, 617 (2004) 1251 [arXiv:astro-ph/0401311].
- [91] A. Tiengo, et al., *A&A*, 423 (2004) 861 [arXiv:astro-ph/0402644].
- [92] J. Hjorth, et al., *ApJ*, 848 (2017), L31 [arXiv:1710.05856].
- [93] S. Dado, A. Dar, 2017 [arXiv:1708.04603].
- [94] A.G. Riess, et al., *ApJ*, 826 (2016) 56 [arXiv:1604.01424].  
A.G. Riess, et al. (2018) [arXiv:1804.10655].
- [95] I. Mandel, *ApJ*, 853 (2018), L12 [arXiv:1712.03958].  
S. Nissanke, et al., *ApJ*, 725, (2010) 496 [arXiv:0904.1017].
- [96] A. Goldstein, et al., *ApJ*, 848 (2017) L14 [arXiv:1710.05446].
- [97] R. Margutti, et al., *ApJ*, 848 (2017) L20 [arXiv:1710.05431].  
E. Troja, et al., *GCN* 22201 (2017).  
R. Margutti, et al., *GCN* 22203 (2017).  
E. Troja, et al., *Nature*, 551 (2017) 71 [arXiv:1710.05433].  
D. Haggard, M. Nynka, J.J. Ruan, 2018, *GCNs* 23137, 23140 (2018).
- [98] G. Hallinan, et al., *Science*, 358 (2017) 1559 [arXiv:1710.05435].  
K.P. Mooley, et al., *Nature* 554 (2018) 207 [arXiv:1711.11573V1].  
K.P. Mooley, et al., 2018 [arXiv:1806.09693].  
K. Hotokezaka, et al., 2018 [arXiv:1806.10596].  
D. Dobie, K. Mooley, T. Murphy, *GCN Circ.* 23139 (2018).
- [99] G.P. Lamb et al., 2018 [arXiv:1811.11491V2].
- [100] K.P. Mooley, et al., [arXiv:1711.11573V1].
- [101] D. Dobbie et al. *ApJ* 858 (2018) L15 [arXiv:1803.06853V3].
- [102] K.P. Mooley, et al., *ApJ*, 868 (2018), L11 [arXiv:1810.12927].
- [103] K. Beuermann, et al., 1999, *A&A*, 352, L26 (Ref. [70]).
- [104] R. Sari, et al., *ApJL*, 497 (1998) L17 [arXiv:astro-ph/9712005].
- [105] D. Lazzati, et al., 2017 arXiv:1712.03237v1.
- [106] D. Lazzati, et al., *PRL*, 120 (2018) 241103 [arXiv:1712.03237v4].

TABLE III: Critical Tests of The Cannonball and Fireball models of GRBs and SHBs

Test	Cannonball Model		Fireball Model	
Test 1	Large GRB Linear Polarization	<b>V</b>	Small GRB Polarization	<b>X</b>
Test 2	Prompt Emission Correlations	<b>V</b>	Frail Relation	<b>X</b>
Test 3	Univ. Shape of GRB Pulses	<b>V</b>	Curvature Radiation	<b>X</b>
Test 4	SN-GRBs: Canonical Afterglow	<b>V</b>	Canonical AG not expected	<b>X</b>
Test 5	AG break-time correlations	<b>V</b>	AG break-time correlations	<b>X</b>
Test 6	Post Break Closure Relation	<b>V</b>	Post break Closure Relation	<b>X</b>
Test 7	Missing Breaks (Too Early)	<b>V</b>	Missing Breaks (Too Late)	<b>X</b>
Test 8	Predicted Chromatic Behavior	<b>V</b>	Achromatic behavior Predicted	<b>X</b>
Test 9	SN-less GRBs:Universal MSP AG	<b>V</b>	Magnetar Jet re-energization	<b>X</b>
Test 10	GRB Rate $\propto$ SFR	<b>V</b>	GRB Rate not $\propto$ SFR	<b>X</b>
Test 11	LL GRBs = Far Off-axis GRBs	<b>V</b>	LL GRBs = Different GRB class	<b>X</b>
Test 12	Super luminal CBs	<b>V</b>	Superluminal Image Expansion	<b>X</b>
Test 13	Properties of SHB170817A	<b>V</b>	Properties of SHB170817A	<b>X</b>

TABLE IV: Majority and minority views on GRBs before decisive observational evidence

Key property	Majority View		Minority View	
GRB Location	Galactic	X	Extragalactic	V
GRBs Produced By	Relativistic Fireballs	X	Highly Relativistic Jets	V
GRB Pulses from	Collisions of $e^+e^-$ shells	X	ICS of External Light by plasmoids	V
Emission Geometry	Isotropic	X	Narrowly Beamed	V
Afterglow Origin	Shocked ISM	X	Synchrotron From ISM Swept Into Jet	V
Afterglow Distribution	Isotropic	X	Narrowly Beamed	V
LGRBs Origin	SN-Less Collapse to BH	X	Stripped Envelope SN	V
SN1998bw/GRB980425	Rare SN/Rare GRB	X	SNIc-GRB Viewed Far Off-Axis	V
LL GRBs	Different class of GRBs	X	Ordinary GRBs Viewed Far Off-Axis	V
SN-Less LGRBs	SN-Less Collapse to BH	X	$n^*$ to $q^*$ phase transition in HMXBs	V
Prompt Emission	Synchrotron	X	Inverse Compton	V
Origin of Jet break	Conical Jet Deceleration	X	Plasmoid Deceleration by Swept-in ISM	V
Rate of GRBs	$\propto$ SFR + Evolution	X	$\propto$ SFR + beaming	V
AG plateau (SN-GRBs)	Jet Re-energization	X	Jet Deceleration at Early Time	V
AG plateau(SN-less GRBs)	Jet Re-energization	X	PWN Emission Powered by MSP	V
Missing Jet Breaks	After AG Observations End	X	Before AG Is Observable	